Characterization of the CLASP2 Protein Interaction Network Identifies SOGA1 as a Microtubule-Associated Protein*[S]

Rikke Kruse‡§, James Krantz¶, Natalie Barker¶, Richard L. Coletta‖, Ruslan Rafikov¶, Moulun Luo¶, Kurt Højlund‡§, Lawrence J. Mandarino¶, and Paul R. Langlais¶**

CLASP2 is a microtubule-associated protein that undergoes insulin-stimulated phosphorylation and co-localization with reorganized actin and GLUT4 at the plasma membrane. To gain insight to the role of CLASP2 in this system, we developed and successfully executed a streamlined interactome approach and built a CLASP2 protein network in 3T3-L1 adipocytes. Using two different commercially available antibodies for CLASP2 and an antibody for epitope-tagged, overexpressed CLASP2, we performed multiple affinity purification coupled with mass spectrometry (AP-MS) experiments in combination with label-free quantitative proteomics and analyzed the data with the bioinformatics tool Significance Analysis of Interactome (SAINT). We discovered that CLASP2 coimmunoprecipitates (co-IPs) the novel protein SOGA1, the microtubule-associated protein kinase MARK2, and the microtubule/actin-regulating protein G2L1. The GTPase-activating proteins AGAP1 and AGAP3 were also enriched in the CLASP2 interactome, although subsequent AGAP3 and CLIP2 interactome analysis suggests a preference of AGAP3 for CLIP2. Follow-up MARK2 interactome analysis confirmed reciprocal co-IP of CLASP2 and revealed MARK2 can co-IP SOGA1, glycogen synthase, and glycogenin. Investigating the SOGA1 interactome confirmed SOGA1 can reciprocal co-IP both CLASP2 and MARK2 as well as glycogen synthase and glycogenin. SOGA1 was confirmed to colocalize with CLASP2 and with tubulin, which identifies SOGA1 as a new microtubule-associated protein. These results introduce the metabolic function of these proposed novel protein networks and their relationship with microtubules as new fields of cytoskeleton-associated protein biology. ***Molecular & Cellular Proteomics 16: 10.1074/mcp.RA117.000011, 1718–1735, 2017.***

Microtubules are versatile cytoskeletal structures known to serve the needs of the particular subcellular context they are situated in. Whether they act as a cellular highway tasked with the trafficking of molecular cargo to specific destinations or function to support the structure of the cell, proper microtubule dynamics are essential for normal cell function. The insulin-stimulated glucose uptake system has distinct effects on the cytoskeleton. Insulin mediates acute glucose uptake in part by mobilizing insulin-stimulated glucose transporter 4 (GLUT4)[1] storage vesicles (GSVs) from intracellular pools to the plasma membrane. Insulin stimulates actin to reassemble into filamentous cortical projections, resulting in the physical effect of ruffling the plasma membrane. Insulin signaling proteins such as WASP, Arp3, PI 3-K, Akt, GLUT4, and additional proteins all colocalize with reorganized actin at the membrane ruffle (1–3). Inhibition of actin reorganization with the drugs

From the ‡The Section of Molecular Diabetes & Metabolism, Department of Clinical Research and Institute of Molecular Medicine, University of Southern Denmark, DK-5000 Odense, Denmark; §Department of Endocrinology, Odense University Hospital, DK-5000 Odense, Denmark; ¶Department of Medicine, Division of Endocrinology, University of Arizona College of Medicine, Tucson, Arizona 85721; ‖School of Life Sciences, Arizona State University, Tempe, Arizona 85787

Received March 31, 2017

Published, MCP Papers in Press, May 26, 2017, DOI 10.1074/mcp.RA117.000011

Author contributions: R.K., J.K., N.B., R.R., M.L., L.J.M., and P.R.L. performed research; R.K., J.K., R.L.C., R.R., M.L., K.H., L.J.M., and P.R.L. analyzed data; R.K., J.K., R.R., M.L., K.H., L.J.M., and P.R.L. wrote the paper; J.K., M.L., K.H., L.J.M., and P.R.L. designed research; R.L.C., R.R., M.L., L.J.M., and P.R.L. contributed new reagents/analytic tools.

[1] The abbreviations used are: GLUT4, glucose transporter 4; AP-MS, affinity purification coupled with mass spectrometry; AGAP1, Arf-GAP with GTPase; ANK, repeat and PH domain-containing protein 1; AGAP3, Arf-GAP with GTPase; ANK, repeat and PH domain-containing protein 3; BLAST, Basic Local Alignment Search Tool; CLASP1, CLIP-associating protein 1; CLASP2, CLIP-associating protein 2; CLIP1/CLIP-170, CAP-Gly domain-containing linker protein 1; CLIP2/CLIP-115, CAP-Gly domain-containing linker protein 2; co-IP(s), co-immunoprecipitation(s); FA, formic acid; GAP, GTPase-activating protein; GAS2L1/G2L1, GAS2 like protein 1; GFP, green fluorescent protein; GLYG, glycogenin; GYS1, glycogen synthase; GSV(s), GLUT4 storage vesicle(s); HA, hemagglutinin; ID, identification; INS, insulin; IP(s), immunoprecipitation(s); MARK2, microtubule affinity-regulating kinase 2; MARK3, microtubule affinity-regulating kinase 3; MK, protein ladder marker; MTOC, microtubule organization center; NIgG, nonimmune serum; PI 3-K, phosphoinositide 3-kinase; P-Score, probability score; SAINT, Significance Analysis of Interactome; SD, standard deviation; SOGA1, suppressor of glucose by autophagy; SCP, Spectrum Count Profile; TIRFM, total internal reflection fluorescence microscopy; TGN, *trans*-Golgi network; TUG/ASPC1, Tether containing UBX domain for GLUT4; WCL, whole cell lysate; YASARA, Yet Another Scientific Artificial Reality Application.

latrunculin B and jasplakinolide in 3T3-L1 adipocytes (4, 5), L6 myotubes (1, 6), rat adipocytes (7), and rat skeletal muscle (8) supports the dependence of insulin-stimulated GLUT4 translocation and glucose uptake on actin reorganization. Conversely, microtubules undergo rapid depolymerization and polymerization cycles, resulting in the shortening and lengthening of the microtubule, which is assisted by microtubule associating proteins (9). Total internal reflection fluorescence microscopy (TIRFM) revealed that microtubules respond to insulin stimulation with a substantial increase in microtubule density and curvature directly underneath the plasma membrane (10). Long range movement of GSVs along microtubules has been established (11, 12) and real-time TIRFM in living 3T3-L1 adipocytes proved insulin-stimulated fusion of GSVs occurs proximal to microtubules at the plasma membrane. Nonspecific inhibition of the kinesin motor protein family (13), and later the conventional kinesin KIF5B (14) and KIF3 (15), which transport vesicles outwards toward the growing plus end of the microtubule, decreased detection of GLUT4 at the cell surface in response to insulin. However, nocodazole-induced disassembly of microtubules did not significantly decrease the number of GSV fusion events stimulated by insulin, leading to the hypothesis that microtubules are not vital for the insertion of GSVs into the plasma membrane, but rather play a more important role in site selection for delivery of GLUT4 prior to fusion (10). Even with these substantial discoveries, the function of the insulin-stimulated effects on the cytoskeleton in GLUT4 trafficking and glucose uptake are completely unknown.

CLIP-associating protein 2 (CLASP2), a member of the plus-end tracking microtubule-associated protein family, was recently linked to acute insulin action (16). The CLASPs (CLASP1 and CLASP2), discovered in 2001 as binding partners for the CAP-Gly domain-containing linker proteins 1 and 2 (CLIP1/CLIP-170 and CLIP2/CLIP-115), were initially found to bind and stabilize the growing, distal ends of microtubules, independently of the CLIPs (17). Subsequent studies revealed that CLASPs localize wherever microtubules are needed, kinetochores in the nucleus for mitosis (18–23), the cell cortex (24–27), the leading edge lamella and lamellipodium of motile cells (28–31), the Golgi (17, 32–38), axons (39, 40), the developing apical membrane surface during lumen formation within endothelial cells (41), adherens junctions at cell-cell contacts (42, 43), the neuromuscular junction (44–46), podosomes (47), and focal adhesions (48). Within each of these molecular systems, the dynamic instability of microtubules undergo differential regulation by proteins specific to each of the biological processes (49–55). In the insulin signaling pathway only a few microtubule-associated proteins, CLASP2 (16) and PHLDB2/LL5α (56) for example, have been associated with insulin stimulation although the defined role of these proteins and microtubules in insulin-stimulated glucose uptake is not understood.

The adipocyte has the distinct property of storing large amounts of lipid, secretion of several hormones, and in addition, serves as a secondary site for insulin-stimulated glucose uptake and storage (57). Knockdown of CLASP2 protein expression in 3T3-L1 adipocytes inhibited insulin-stimulated glucose transport (16). Here we report label-free quantification of interactome experiments that have been processed with the Significance Analysis of Interactome (SAINT) scoring system (58–61). By performing a series of strategic, successive and confirmatory reciprocal interactome experiments on key novel proteins, we have constructed a 3T3-L1 adipocyte CLASP2 protein network that has led to the identification of suppressor of glucose by autophagy 1 (SOGA1) as a microtubule-associated protein.

EXPERIMENTAL PROCEDURES

Cell Culture, Immunoprecipitation, and Western Blot Analysis—3T3-L1 fibroblasts were cultured in growth media of DMEM (Thermo Fisher Scientific, Waltham, MA, cat. # SH30243.01) with 10% newborn calf serum (Thermo Fisher Scientific, cat. # 16010), 1% penicillin-streptomycin (Thermo Fisher Scientific, cat. # 15140), and 1% glutamax (Thermo Fisher Scientific, cat. # 35050) until confluence. After changing to fresh growth media and culturing for 48 h, differentiation day one was initiated by changing to differentiation media: DMEM with 10% fetal bovine serum (Thermo Fisher Scientific, cat. # 16000), 1% penicillin-streptomycin, and 1% glutamax supplemented with 10.0 μg/ml insulin (Sigma-Aldrich, cat. # I-2643), 0.5 mM IBMX (Sigma-Aldrich, cat. # I-5879), and 1.0 μM dexamethasone (Sigma-Aldrich, cat. # D-1756). After 48 h, differentiation media supplemented with only 10.0 μg/ml insulin was added. After 48 h of culturing in this media, fresh differentiation media with no supplements was added every 24–48 h until lysis, which was performed on day 7 or 8 post-differentiation. For cell treatment experiments, cells were starved for 4 h and then either left untreated or stimulated with 100 nM insulin for 15 min at 37 °C. Cells were lysed with 500 μl of lysis buffer containing 40 mM HEPES (pH 7.6), 120 mM NaCl, 0.3% CHAPS, 10 mM NaF, 10 mM β-glycerol phosphate, 1 mM EDTA (pH 8.0), 2 mM sodium orthovanadate, 17 μg/ml aprotinin, 10 μg/ml leupeptin, and 1 mM PMSF. Cell lysates were rotated at 4 °C for 20 min followed by centrifugation (14,000 RPM, 4 °C, 20 min), and the clarified supernatants were used for immunoprecipitation (IP). For each IP, cell lysate from 1 $\times$ 150 mm tissue culture dish ($\sim$3.5–5 mg) was incubated with 5 μg of specific antibodies conjugated to 25 μl protein A or protein G-agarose beads for 3 h at 4 °C with gentle rotation. IPs were washed three times with 1 ml of ice-cold PBS and the proteins bound to beads were eluted by heating at 95 °C for 4 min in 8 μl SDS sample loading buffer (4%SDS, 0.0625 M Tris-HCl, 10% glycerol, 0.02% bromphenol blue, 8 M Urea). The eluate was extracted and the antibody/beads were subjected to a second elution at 95 °C for 4 min in 8 μl SDS sample loading buffer. The second eluate was extracted and the two eluates were combined and separated by 10% SDS-PAGE and the gels were either stained with Bio-Safe Coomassie G-250 Stain (Bio-Rad, Hercules, CA) or transferred to a nitrocellulose membrane for subsequent Western blotting. For Western blots, proteins were transferred to a nitrocellulose membrane for 1 h at 105 V and blocked with 5% nonfat dry milk in Tris-buffered saline with 0.2% Tween-20 for 1 h at room temperature. Membranes were probed with primary antibodies for 1 h in blocking buffer at room temperature. Blots were washed in Tris-buffered saline with 0.2% Tween-20 (three times for 10 min), and probed with either goat anti-mouse (Santa Cruz Technologies, Santa Cruz, CA) or donkey anti-rabbit (GE Healthcare, Waukesha, WI)

secondary antibodies (both at dilutions of 1:1500) conjugated to horseradish peroxidase and detected with Western Lightning Plus-ECL Enhanced Chemiluminescence Substrate kit (Perkin Elmer, Waltham, Massachusetts). Primary antibodies used: anti-CLASP2 "Antibody #1" (the immunogen recognized by this antibody maps to a region between residue 275 and 325 of human CLASP2 using the numbering given in entry BAG11221.1 (GeneID 23122), cat. # 21395, Novus Biologicals, Littleton, CO), anti-CLASP2 "Antibody #2" (immunogen not supplied by manufacturer, cat. # ABT263, Millipore, Billerica, MA), anti-CLIP2 (cat. # SAB1412760, Sigma-Aldrich), anti-MARK2 (cat. # NBP1–71890, Novus Biologicals), anti-SOGA1 (cat. # SAB3500961, Sigma-Aldrich), anti-AGAP3 (cat. # SAB2700915, Sigma-Aldrich), anti-HA (cat. # 901501, Biolegend, San Diego, CA), anti-mCherry (cat. # NBP2–43720, Novus Biologicals), anti-tubulin (cat. # T9026, Sigma-Aldrich and cat. # ab18251, abcam, Cambridge, MA).

In-gel Digestion—Proteins were separated by SDS-PAGE and stained with Bio-Safe Coomassie G-250 Stain. For the interactome experiments, each lane of the SDS-PAGE gel was cut into either seven or eight slices (the number of slices was consistent for each specific protein's interactome), placed in a 0.6 ml LoBind polypropylene tube (Eppendorf, Hauppauge, NY), destained twice with 375 μl of 50% acetonitrile (ACN) in 40 mm NH_4HCO_3 and dehydrated with 100% ACN for 15 min. After removal of the ACN by aspiration, the gel pieces were dried in a vacuum centrifuge at 60 °C for 30 min. Trypsin (250 ng; Sigma-Aldrich) in 20 μl of 40 mm NH_4HCO_3 was added, and the samples were maintained at 4 °C for 15 min prior to the addition of 50–100 μl of 40 mm NH_4HCO_3. The digestion was allowed to proceed at 37 °C overnight and was terminated by addition of 10 μl of 5% formic acid (FA). After further incubation at 37 °C for 30 min and centrifugation for 1 min, each supernatant was transferred to a clean LoBind polypropylene tube. The extraction procedure was repeated using 40 μl of 0.5% FA, and the two extracts were combined and dried down to ~5–10 μl followed by the addition of 10 μl 0.05% heptafluorobutyric acid/5% FA (v/v) and incubation at room temperature for 15 min. The resulting peptide mixtures were loaded on a solid phase C18 ZipTip (Millipore, Billerica, MA) and washed with 35 μl 0.005% heptafluorobutyric acid/5% FA (v/v) followed by elution first with 4 μl of 50% CAN/1% FA (v/v) and then a more stringent elution with 4 μl of 80% ACN/1% FA (v/v). The eluates were combined and dried completely by vacuum centrifugation and 6 μl of 0.1% FA (v/v) was added followed by sonication for 2 min. 2.5 μl of the final sample was then analyzed by mass spectrometry.

Mass Spectrometry and Data Processing—HPLC-ESI-MS/MS was performed in positive ion mode on a Thermo Scientific Orbitrap Elite Velos Pro hybrid mass spectrometer fitted with an EASY-Spray Source (Thermo Scientific, San Jose, CA). NanoLC was performed using a Thermo Scientific UltiMate 3000 RSLCnano System with an EASY Spray C18 LC column (Thermo Scientific, 50 cm × 75 μm inner diameter, packed with PepMap RSLC C18 material, 2 μm, cat. # ES803); loading phase for 15 min; mobile phase, linear gradient of 1–47% ACN in 0.1% FA in 106 min, followed by a step to 95% ACN in 0.1% FA over 5 min, hold 10 min, and then a step to 1% ACN in 0.1% FA over 1 min and a final hold for 19 min (total run 156 min); Buffer A = 100% H_2O in 0.1% FA; Buffer B = 100% ACN in 0.1% FA; flow rate, 300 nl/min. All solvents were liquid chromatography mass spectrometry grade. Spectra were acquired using XCalibur, version 2.1.0 (Thermo Scientific). A "top 15" data-dependent MS/MS analysis was performed (acquisition of a full scan spectrum followed by collision-induced dissociation mass spectra of the 15 most abundant ions in the survey scan). Dynamic exclusion was enabled with a repeat count of 1, a repeat duration of 30 s, an exclusion list size of 500, and an exclusion duration of 40 s. Tandem mass spectra were extracted from Xcalibur "RAW" files and charge states were assigned using the ProteoWizard 2.1.x msConvert script using the default parameters (62). The fragment mass spectra were then searched against the mouse SwissProt_2015_08 database (16,724 entries) using Mascot (Matrix Science, London, UK; version 2.5.0) using the default probability cut-off score. The search variables that were used were: 10 ppm mass tolerance for precursor ion masses and 0.5 Da for product ion masses; digestion with trypsin; a maximum of two missed tryptic cleavages; variable modifications of oxidation of methionine and phosphorylation of serine, threonine, and tyrosine. Cross-correlation of Mascot search results with X! Tandem was accomplished with Scaffold (version Scaffold_4.4.0; Proteome Software, Portland, OR), and the Scaffold reported decoy false discovery rate across all sixteen samples in the CLASP2 Antibody #1 interactome experiments was 0.19%, which is representative of typical rates calculated throughout the remainder of the interactome experiments. Probability assessment of peptide assignments and protein identifications were made using Scaffold. Only peptides with ≥ 95% probability were considered. The mass spectrometry proteomics data have been deposited to the ProteomeXchange Consortium (http://proteomecentral.proteomexchange.org) via the PRIDE partner repository (63) with the data set identifier PXD003674.

Cloning and Subcloning Mouse CLASP2—Total RNA was isolated from the homogenized brain of a C57BL/6J mouse according to the manufacturer's protocol (RNeasy Mini Kit, cat. # 74104, Qiagen). RT-PCR was utilized to convert mRNA into single-stranded cDNA following the manufacturer's protocol (LongRange 2Step RT-PCR Kit, cat. # 205922, Qiagen). The total cDNA was used to amplify cDNA with specific primers by PCR and then amplified cDNA was inserted into a vector. For cloning of mouse CLASP2 cDNA, the sense primer was 5′-ggccatgtgaactattaggagctattctagggtg-3′ and antisense primer 5′-gcagccagttgtcctctcagagactgggaggcg-3′. Sequencing results reveal that the cloned CLASP2 cDNA has the same sequence as NM_001081960.1. This cDNA was subcloned and inserted into the pCMV6-AN-HA plasmid (Origene, Rockville, MD, cat. # PS100013) to generate the construct pCMV-HA-CLASP2. The construct was verified by restriction digestion and DNA sequencing.

Generation of Adenoviruses and Adenoviral Infection of 3T3-L1 Adipocytes—Negative control null adenovirus and GFP/HA-tagged mouse CLASP2 adenovirus (using the aforementioned pCMV-HA-CLASP2 vector to generate N-terminal GFP and C-terminal HA-tagged CLASP2) were created by VECTOR BIOLABS (Malvern, PA). Negative control null adenovirus and mCherry-tagged mouse MARK2 adenovirus (mouse MARK2 cDNA, cat. # MC204604, was purchased from Origene) were also created by VECTOR BIOLABS. Virus infections were performed on 150 mm plates of 3T3-L1 adipocytes after 7–8 days of differentiation as described above. After one PBS wash, 10 ml of serum-free DMEM containing 8.5×10^8 PFUs of virus and 5.0 μg/ml polybrene was added to each plate followed by incubation at 37 °C for 4 h. Fifteen milliliters of serum-containing DMEM was then added to each plate followed by incubation at 37 °C for 48 h. Cells were then serum-starved for 4 h followed by insulin treatment and cell lysis as described above.

Immunofluorescence and Confocal Microcopy—3T3-L1 adipocytes grown on #1.5H coverslips (Zeiss, Thornwood, NY, cat. # 474030-9000-000,) were fixed in methanol at −20 °C for 20 min, permeabilized at room temperature with 1% Tween-20/2% paraformaldehyde solution for 20 min, quenched at room temperature with 0.1 M glycine for 20 min, blocked at room temperature with 1% BSA for 2 × 15 min (IgG-free, protease-free, Jackson Immunoresearch cat. # 001-000-161), and then either left untreated or incubated with primary antibodies overnight at 4 °C with gentle rocking. After 3 × 10 min 1% BSA washes at room temperature, the samples were incubated with either Alexa Fluor 405 Goat anti-mouse (Thermo Fisher cat. # A31553) or Alexa Fluor 647 Goat anti-rabbit (Thermo Fisher cat. # A21245) for 1 h at room temperature with gentle rocking followed by 2 × 10 min

washes in 1% BSA and 2 × 10 min washes in PBS at room temperature. Coverslips were then mounted with ProLong Diamond (Thermo Fisher cat. # P36970). Imaging was conducted using a Zeiss LSM880 Laser Scanning Confocal Microscope housed at the University of Arizona Imaging Cores - Marley Light Microscopy Facility. Multiple lasers (diode 405 nm; argon 488 nm; DPSS 561 nm; and He/Ne 633 nm) allowed for sequential imaging using either a PlanApo 40× or 63× oil objective. Images were scanned at multiple intervals within the *z* axis. The post-acquisition image processing was performed using the Zeiss ZEN Blue software package and Adobe Photoshop software (Mountain View, CA) and best fit max projections are shown.

SOGA1 Homology Modeling—Briefly, a PSI-BLAST in YASARA was used to select the best scored protein templates in the Protein Data Bank of available crystal structures, which was determined to be the crystal structure of the human Cytoplasmic Dynein 2 Motor Domain (PDB ID 4RH7) (64). To reconstruct regions of SOGA1 nonhomologous to 4RH7, BLAST was used to retrieve homologous sequences, create a multiple sequence alignment, and enter the sequences into a "discrimination of secondary structure class" prediction algorithm. The side chain loops were then optimized and added. The resulting structure was subjected to a combined steepest descent algorithm and refined with simulated annealing minimizations within surrounding water.

Experimental Design and Statistical Rationale—Using the mean and standard deviations for the spectrum counts of the 39 proteins identified by SAINT analysis as significantly enriched between the CLASP2 Antibody #1 IPs (Group 1, 343 ± 280) and the NIgG IPs (Group 2, 26 ± 21), the effect size is equal to 1.60. With this robust effect size, a sample size of four biological replicates per group provided more than sufficient power to detect differences between groups. Based on the high degree of reproducibility, we also used a sample size of two and three biological replicates. Each IP had a respective NIgG or appropriate tag antibody negative control IP, two to four biological replicates each, and no process and technical replicates because of the strong reproducibility of the data. The varying statistical analyzes for the different experiments are listed in the Figure Legends and were justifiable based upon the data and basic experiment performed. For spectral counting measurements, modified peptides, semitryptic peptides, and shared peptides were included.

RESULTS

The CLASP2 Interactomes—We devised a streamlined, label-free proteomic technique to identify and quantify protein interaction partners and applied this system to discover proteins that may be linked to regulation of the microtubule-associated protein CLASP2. This method combined cell lysis with a CHAPS detergent-containing buffer together with IP, SDS-PAGE-based fractionation, subsequent in-gel tryptic digestion and bottom-up mass spectrometry analysis (Fig. 1*A*). This approach possesses the caveat that proteins nonspecifically bound to the Sepharose resin, Protein A/G, and nontargeting regions of the antibody are eluted together with the prey proteins, rendering the final interactome sample full of contaminating proteins which need systematic elimination (65, 66). To avoid artifacts resulting from overexpression of epitope-tagged proteins, we used two different commercially available CLASP2 antibodies to independently IP endogenous CLASP2. On the other hand, because antibodies targeted to endogenous protein can disrupt protein-protein interactions and possess nonspecific cross-reactivity (66, 67), we also adenovirally overexpressed HA-epitope and GFP-tagged CLASP2 to create an anti-HA antibody GFP-CLASP2-HA interactome. These three independent CLASP2 interactomes act as cross references, to narrow down the list of potential CLASP2 interaction partners for follow-up confirmation experiments. Western blot of these CLASP2 protein IPs are shown in Figs. 1*B*, 1*C*, and 1*D*. For a detailed breakdown of the proteomic numbers associated with the experimental approach adopted for these interactome studies, using the CLASP2 Antibody #1 experiment numbers as an example, please refer to supplemental Fig. S1 and the accompanying text. For all interactome experiments presented in this study, each gel slice's protein yield, total number of peptides identified, total number of spectra, and percent identification rate are included in supplemental Tables (CLASP2 Antibody #1 data are in supplemental Tables S1, S2, S3, and S4, GFP-CLASP2-HA data are in supplemental Tables S6, S7, S8, and S9, CLASP2 Antibody #2 data are in supplemental Tables S11, S12, S13, and S14). These numbers are provided throughout the remainder of this report for all interactomes performed. CLIP1 and CLIP2 are the original CLASP associated proteins (17), so we chose to use CLIP2 as a high-confidence CLASP2 interacting partner to test the validity of the current experimental conditions and approach, using the CLASP2 Antibody #1 interactome data as an example. Western blot analysis of CLIP2 in the CLASP2 Antibody #1 basal and insulin IPs showed strong enrichment of CLIP2 in the CLASP2 Antibody #1 IPs, with no effect of insulin on the interaction (supplemental Fig. S2*A*, and densitometry results from co-IP/Western blot experiments are shown in supplemental Fig. S2*B*). The spectral count data (supplemental Fig. S2*C*) is very similar to the results from the co-IP/Western blot experiments, in that CLIP2 shows a strong enrichment in the CLASP2 Antibody #1 basal and insulin IPs over the NIgG negative controls and no effect of insulin on the interaction. CLIP2 averaged 134 spectral counts *versus* only 13 for CLIP1 (CLIP1 lacked an effect of insulin as well). The strong co-IP of CLIP2 with CLASP2 supports the validity of the experimental conditions used.

We used the established bioinformatic tool Significance Analysis of Interactome (SAINT) (58–61) to analyze our interactome data for protein enrichment. SAINT assigns each protein a SAINT Probability Score ("P-Score"), on a scale of 0 to 1, with 1 being the top score. Based upon review of the literature, we chose 0.65 as a SAINT cut-off score for enrichment (68–73). With the approach used here, all proteins have two P-Scores, one each for basal or insulin enrichment over the respective negative controls. A detailed breakdown of SAINT results typical for our interactome approach are outlined in supplemental Fig. S3, again using CLASP2 Antibody #1 interactome data as an example. Protein SAINT scores and spectrum counts for all interactomes performed in this study are included in Supplemental Tables (CLASP2 Antibody #1 in

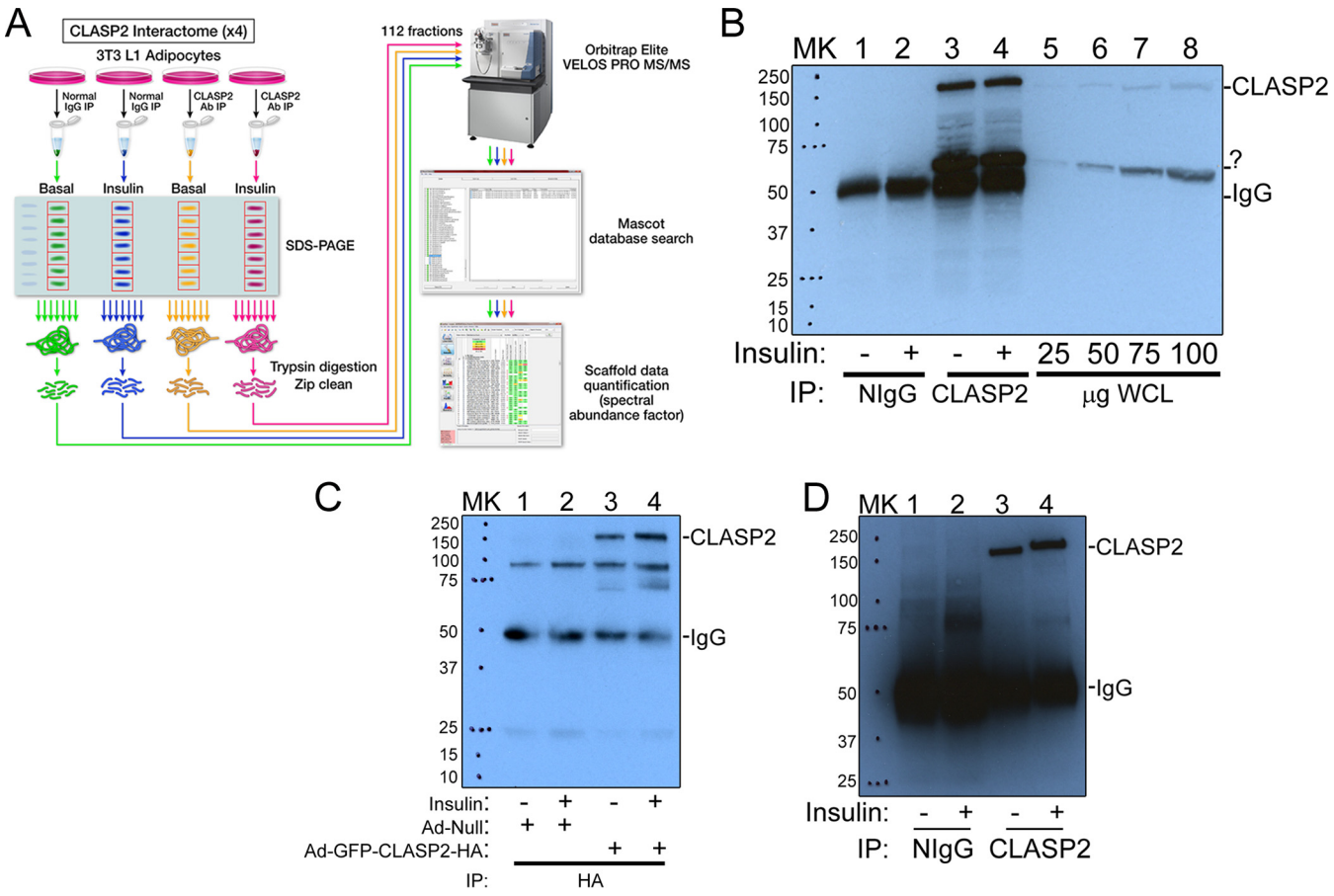

FIG. 1. **The CLASP2 immunoprecipitations.** *A*, The focus of this project was to identify new interacting partners for CLASP2 in 3T3-L1 adipocytes. The approach compared different protein IPs (for this figure, CLASP2) against negative control IPs (for this figure, Nonimmune serum "NIgG"), either in the absence or presence of insulin treatment. The IPs were separated by SDS-PAGE, fractionated into gel slices, subjected to trypsin digestion, and analyzed by tandem mass spectrometry. Peptide and protein identification was performed by database searching with Mascot, and the resulting spectral count data was assembled with Scaffold. *B*, 150 mm plates of serum-starved, differentiated 3T3-L1 adipocytes were either left untreated or treated with 100 nM insulin for 15 mins. The cells were lysed in an isotonic CHAPS lysis buffer and both the NIgG and CLASP2 Antibody #1 IPs were performed as described under Experimental Procedures. The IPs or whole cell lysates (WCL) were resolved by 10% SDS-PAGE and transferred to nitrocellulose membranes. The membranes containing the immunoprecipitated proteins were subjected to Western blot with CLASP2 Antibody #1. The labels on the right side of the blot indicate where CLASP2 and the heavy chain IgG migrate on the gel, and the question mark ("?") points out a prominent nonspecific band. "MK" stands for protein ladder marker. *C*, 150 mm plates of differentiated 3T3-L1 adipocytes were infected with either null GFP adenovirus or GFP-CLASP2-HA adenovirus as described under Experimental Procedures. The cells were serum starved and either left untreated or treated with 100 nM insulin for 15 mins. The cells were lysed and the lysates were subjected to anti-HA IP and Western blot and using the same procedure for CLASP2 Antibody #1 as described above. *D*, The CLASP2 Antibody #2 experiment was performed in a similar manner as described above for the CLASP2 Antibody #1 experiment.

supplemental Table S5, GFP-CLASP2-HA data in supplemental Table S10, CLASP2 Antibody #2 data in supplemental Table S15).

We sought to analyze the raw spectral count data of all proteins with SAINT scores greater than a 0.65 in both the basal and insulin samples (which we refer to as "SAINT-qualified") in a hierarchical manner, with spectral count results from all experiments individually plotted. We therefore devised the Spectrum Count Profile (SCP), an easily readable format for the visualization of whole sets of raw spectral count data for interactome experiments, and applied it to the CLASP2 Antibody #1 interactome data (Fig. 2*A*). Using the same interactome processing approach, we generated SCPs for the two remaining CLASP2 interactomes we had prepared as cross references, the adenovirally overexpressed HA-epitope and GFP-tagged CLASP2 anti-HA IP (Fig. 2*B*) and the second, alternative CLASP2 Antibody #2 IP (Fig. 2*C*). We first searched the three SAINT-qualified CLASP2 interactomes for proteins previously linked to CLASP2 (for reviews on CLASP2 and members of the plus-end tracking microtubule-associated protein family, please refer to (49, 51–54, 74)) and found MARE1/EB1, SLAIN2, MARK2, MARK3, CLIP1, CKAP5/ch-TOG, PHLDB1/LL5α, MACF1, GCC2, CLASP1, CLIP1, and CLIP2. The CLASP2 Antibody #1 interactome had more

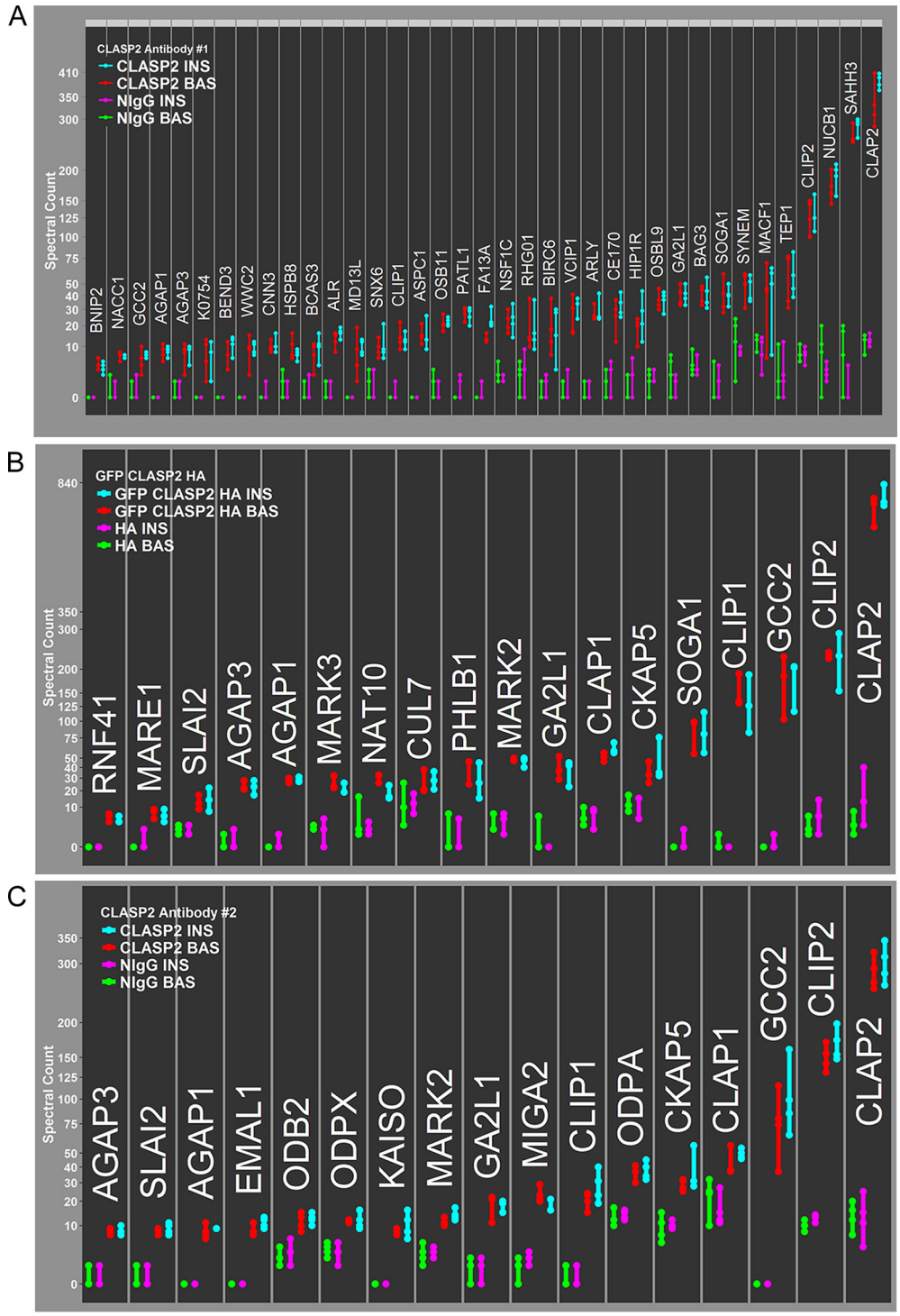

FIG. 2. **SAINT scoring and Spectrum Count Profile analysis of the CLASP2 interactomes.** *A*, For the CLASP2 Antibody #1 IP experiments, the 39 "SAINT-qualified" proteins were ordered in a hierarchical manner, from lowest spectrum counts identified (BNIP2) to highest (CLAP2), and results from all four experiments were individually plotted in a Spectrum Count Profile ("SCP"). Basal NIgG IPs (green), insulin NIgG IPs (magenta), basal CLASP2 Antibody #1 IPs (red), and insulin CLASP2 Antibody #1 IPs (turquoise). *B*, Anti-HA antibody IPs for GFP-CLASP2-HA were performed as described in Fig. 1. Tandem mass spectrometry on the IPs was performed as described under Experimental Procedures ($n = 3$) and SCP analysis of the 18 SAINT-qualified proteins is shown. *C*, CLASP2 Antibody #2 IPs were performed as described in Fig. 1. Tandem mass spectrometry on the IPs was performed as described under Experimental Procedures ($n = 4$) and SCP analysis of the 17 SAINT-qualified proteins is shown.

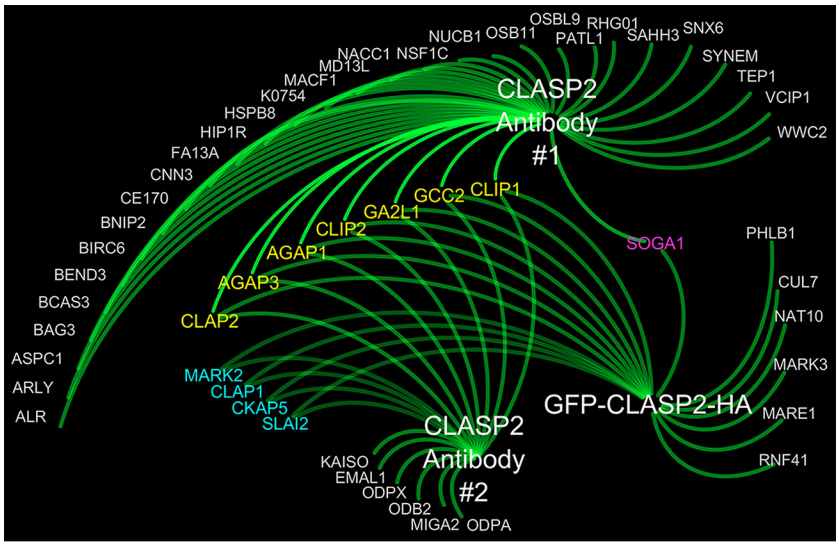

FIG. 3. **Cytoscape-based integrated visual representation of the CLASP2 Antibody #1, GFP-CLASP2-HA, and CLASP2 Antibody #2 interactomes.** The proteins listed in yellow were identified in all three of CLASP2 interactomes, whereas the proteins listed in blue were shared between CLASP2 Antibodies #1 and #2. The protein listed in pink was shared between CLASP2 Antibody #1 and GFP-CLASP2-HA.

SAINT-qualified proteins, although reciprocal co-IP follow-up interactome experiments were unsuccessful for two of these, namely TUG/ASPC1, which we chose because of a reported role in insulin action (75, 76), and FAM13A because this protein exhibited a significant increase in abundance in the CLASP2 IPs upon insulin stimulation (data not shown). TUG and FAM13A were exclusive to the CLASP2 Antibody #1 interactome, so we took advantage of Cytoscape (77) for the integration and visualization of all three CLASP2 interactomes and followed up on SAINT-qualified proteins that were present in more than one of the individual CLASP2 interactomes (Fig. 3). This approach helps overcome false positives resulting from cross-reactivity or nonspecificity from a single antibody. Proteins with established links to CLASP2 that were present in multiple CLASP2 interactomes include the binding partners SLAIN2 and CKAP5/ch-TOG (78), CLASP1, MARK2 (21), GCC2 (also known as GCC185) (32), and of course CLIP1 and CLIP2 (17). In addition, we present the novel discoveries that CLASP2 co-IPs Arf-GAP with GTPase, ANK repeat and PH domain-containing proteins 1 and 3 (AGAP1 and AGAP3), the microtubule/actin-regulating protein GAS2-like protein 1 (GA2L1/G2L1), and the protein "suppressor of glucose by autophagy" (SOGA1), all of which together represent a new subset of CLASP2-associated proteins that do not have any previously established connection to CLASP2.

The AGAP3 and CLIP2 Interactomes—AGAP1, AGAP2, and AGAP3 are GAP proteins with links to membrane traffic and actin (79). Because both AGAP1 and AGAP3 were present in all three CLASP2 interactomes, and GAP proteins are important regulators of cytoskeletal dynamics and vesicle trafficking, we chose to analyze the AGAP3 interactome with a commercially available antibody, using the same SAINT-based interactome approach as described above for CLASP2 (Fig. 4*A* and accompanying supplemental Tables S16, S17, S18, S19, and S20). SCP analysis of the SAINT-qualified AGAP3 interactome confirmed successful immunoprecipitation of AGAP3 and while CLASP1 but not CLASP2 was detected, CLIP2 was highly enriched, as was AGAP1, albeit to a lesser extent. This finding introduced the possibility that AGAP3 was enriched in the CLASP2 interactomes because of binding CLIP2 rather than direct interaction with CLASP2. To test this, we analyzed the CLIP2 interactome with a commercially available antibody, again, using the same interactome approach (Fig. 4*B* and accompanying supplemental Tables S21, S22, S23, S24, and S25). We report the novel finding that AGAP3, and to a lesser extent, AGAP1, can strongly co-IP with CLIP2. Because much less CLASP2 was present in the CLIP2 interactome as compared with the CLASP2 interactomes, and the amount of AGAP3 in the CLIP2 interactome was at least triple the detected levels of AGAP3 in the CLASP2 IPs, these findings suggest a preference of AGAP3 for CLIP2 over CLASP2. To visualize interaction partners shared among CLASP2, CLIP2, and AGAP3, we integrated the corresponding SAINT-qualified interactomes with Cytoscape (Fig. 4*C*). This led to the discovery that G2L1, the novel protein identified in each of the three CLASP2 interactomes, as well as both CKAP5 and SLAIN2, were present in both the CLIP2 and CLASP2 interactomes. This leads to the novel hypothesis that CLIP2-CLASP2-SLAIN2-CKAP5-G2L1 are a protein network, although more evidence is needed supporting a direct link between G2L1, CKAP5 and SLAIN2. Cytoscape integration also revealed that both CLIP2 and AGAP3 share association with CLIP1, CLASP1, and AGAP1, as well as with members of the protein phosphatase 6 holoenzyme, specifically PPP6/PP6C, PP6R3, and ANR28. This could hypothetically act as a second protein network for CLIP2, composed of CLIP2-AGAP3-AGAP1-

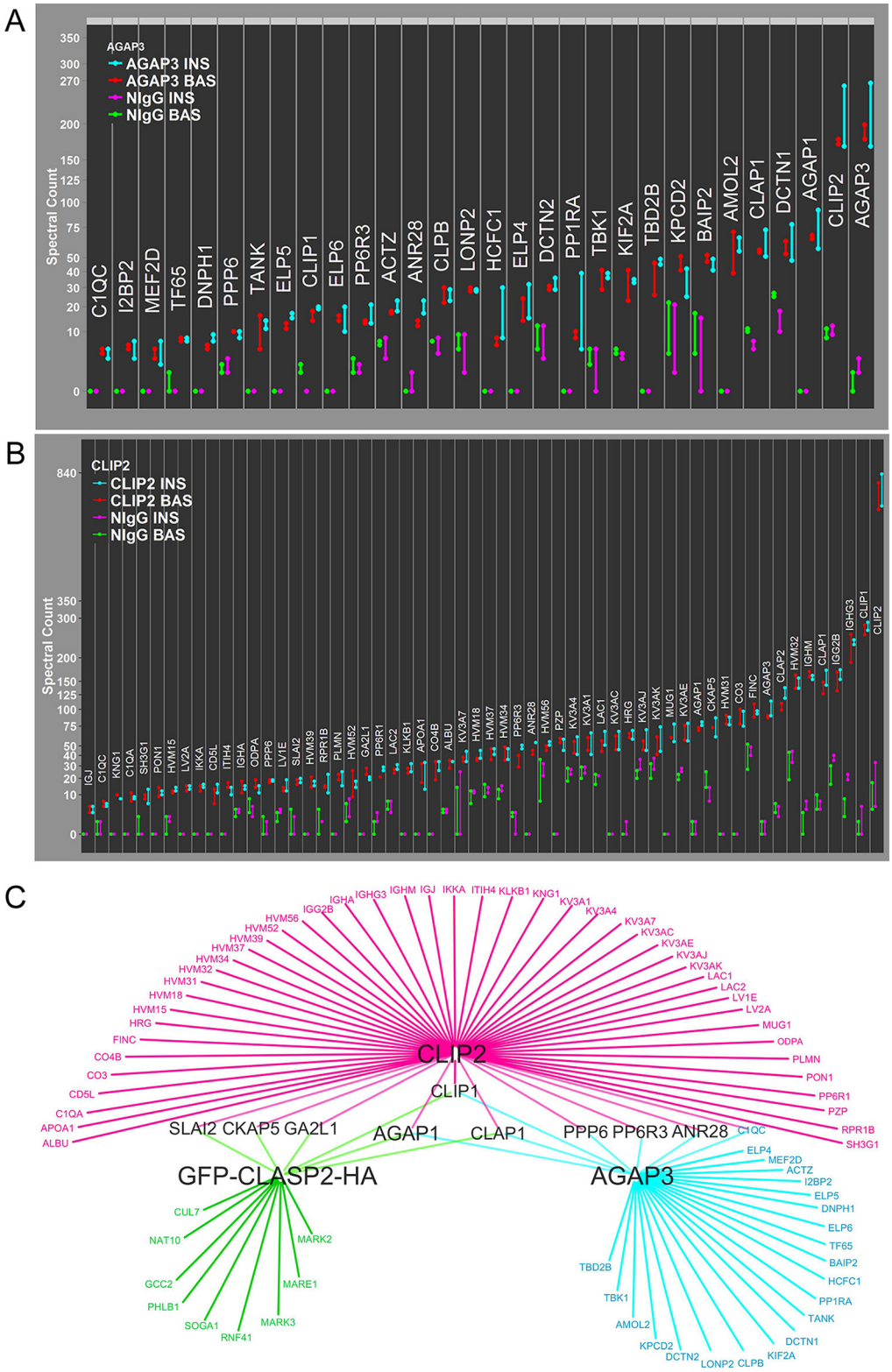

FIG. 4. **SCP analysis for the SAINT-qualified AGAP3 and CLIP2 interactomes and Cytoscape-based CLIP2/AGAP3/GFP-CLASP2-HA interactome integration.** *A*, AGAP3 Antibody IPs and tandem mass spectrometry was performed as described under Experimental Procedures ($n = 2$) and SCP analysis of the 30 SAINT-qualified proteins is shown. *B*, CLIP2 Antibody IPs and tandem mass spectrometry was performed as described under Experimental Procedures ($n = 2$) and SCP analysis of the 58 SAINT-qualified proteins is shown. *C*, Cytoscape-based integrated visual representation of the AGAP3, CLIP2, and GFP-CLASP2-HA interactomes.

PP6C-PP6R3-ANR28. Additional studies will need to address whether the PP6 holoenzyme complex is truly excluded from the CLIP2-SLAIN2-CKAP5 network.

The MARK2 and SOGA1 Interactomes—The MARK family (also known as the Par-1 family) is known to phosphorylate microtubule-associated proteins, which serves to regulate microtubule stability in a negative manner (80), and both MARK2 and MARK3 have been detected by mass spectrometry in GFP-CLASP1 IPs before (21). As a result of the novel discovery of MARK2 in the CLASP2 IPs, we chose to analyze the MARK2 interactome with a commercially available antibody (Fig. 5*A* and accompanying supplemental Tables S26, S27, S28, S29, and S30). SCP analysis of the MARK2 interactome confirmed the successful immunoprecipitation of MARK2 and reciprocal co-IP of CLASP2. The MARK2 interactome also had strong enrichment of glycogen synthase (GYS1) and glycogenin, (GLYG), two proteins vital to the process of glucose storage as glycogen. At 81 SAINT-qualified proteins, this particular MARK2 antibody had the potential for possessing a high degree of nonspecific cross-reactivity. To avoid potential false positives, we created a cross reference MARK2 interactome derived from an adenovirally overexpressed and mCherry-tagged MARK2 immunoprecipitated with an antibody to the mCherry tag (Fig. 5B and accompanying supplemental Tables S31, S32, S33, S34, and S35). SCP analysis of the mCherry-MARK2 interactome revealed 29 SAINT-qualified proteins and confirmed the successful immunoprecipitation of MARK2. The mCherry-MARK2 SAINT score for BAS and INS CLASP2 enrichment was 1 and 0.64, respectively, whereas the BAS and INS SAINT scores for glycogen synthase were 0.9 and 0.4, respectively. When analyzing the spectrum counts for glycogen synthase in the INS samples, the negative control values were 61 and 52 *versus* 537 and 364 in the mCherry-MARK2 IPs, representing a very strong enrichment of GYS1 in the mCherry-MARK2 interactome. We modified the SCP of mCherry-MARK2 to include these two proteins for Cytoscape-based integration of the two MARK2 interactomes (Fig. 5*C*). We confirmed the previous report that MARK2 associates with MTCL1 (81). In addition, suppressor of glucose by autophagy 1 (SOGA1), a protein enriched in two out of the three CLASP2 interactomes, was also identified as a SAINT-qualified protein within both MARK2 interactomes tested. SOGA1 has been linked to adiponectin-mediated inhibition of glucose production by enhancing suppression of autophagy in an insulin-dependent manner in hepatocytes (82), although an association between SOGA1 and microtubules or microtubule-associated proteins has yet to be shown. To test for reciprocal co-IP of CLASP2 and MARK2 with SOGA1, we analyzed the SOGA1 interactome with a commercially available antibody (Fig. 6*A* and accompanying supplemental Tables S36, S37, S38, S39, and S40). SCP analysis of the SOGA1 interactome confirmed both successful immunoprecipitation of SOGA1 and reciprocal co-IP of both CLASP2 and MARK2. Integration of the GFP-CLASP2-HA, SOGA1, and mCherrry-MARK2 interactomes with Cytoscape (Fig. 6*B*) led to the new finding that SOGA1, like MARK2, can co-IP glycogen synthase (GYS1) and glycogenin, (GLYG). As seen in the SCPs for the MARK2 and SOGA1 interactomes, these proteins are coimmunoprecipitating a relatively large amount glycogen synthase. The fact that each of these three unique antibody IPs (SOGA1, MARK2, mCherry-MARK2) are all enriched in glycogen synthase, independent of each other, suggests specificity of this finding.

SOGA1 Colocalizes with CLASP2 and Microtubules—CLASP2 is known to associate with microtubules, a finding that we also show in adipocytes (Fig. 7, top row). Based on the interactome discovery that SOGA1 and CLASP2 can reciprocally co-IP, we hypothesized that SOGA1 and CLASP2 subcellularly colocalize in adipocytes. As shown in Fig. 7 (middle row), in a cell overexpressing CLASP2, both the GFP-CLASP2 and the anti-SOGA1 antibody signals colocalize within microtubule-like heavy bundles, whereas surrounding, non-CLASP2 overexpressing cells show punctate SOGA1 filamentous structures, suggesting SOGA1 may be microtubule-associated. Further analysis directly comparing microtubules (anti-tubulin antibody) and anti-SOGA1 antibody staining (Fig. 7, bottom row) revealed a high degree of SOGA1 and tubulin colocalization, a discovery which identifies SOGA1 as a new microtubule-associated protein.

To follow up on the interactome discoveries of both SOGA1 and CLASP2 potentially linked to the microtubule-associated protein kinase MARK2, we tested for colocalization of MARK2 with CLASP2 and SOGA1. Although GFP-CLASP2 and mCherry-MARK2 showed similar localization, there was a strong loss of microtubule-like structure for CLASP2 (Fig. 8, first row). Similar findings were seen for the anti-SOGA1 and anti-tubulin stains within MARK2 overexpressing cells as well (Fig. 8, second and third rows). These results agree with others who have reported that overexpression of MARK2 disrupts the microtubule network, from a complete loss of microtubules to varying stages of microtubule disruption (80), a phenomenon we reproduced in adipocytes. The lack of SOGA1 colocalizing with tubulin in cells with MARK2 overexpression-induced microtubule destabilization is further evidence that SOGA1 is a microtubule-associated protein. Interestingly, as seen in the overexpressed mCherry-MARK2 interactome (Fig. 5*B*), even with the loss of microtubule integrity, mCherry-MARK2 was still able to strongly co-IP SOGA1 and GYS1, which questions the necessity of intact microtubules for MARK2 to network with SOGA1 and GYS1.

To better understand the SOGA1 structure-function relationship, we developed a homology model of full-length SOGA1 protein structure. Due to the absence of an X-ray crystallography structure for SOGA1, we utilized the YASARA Structure software package (83) to perform three-dimensional homology modeling of SOGA1 (Uniprot Accession E1U8D0) *in silico*. Screening of SOGA1 against the Protein Data Bank

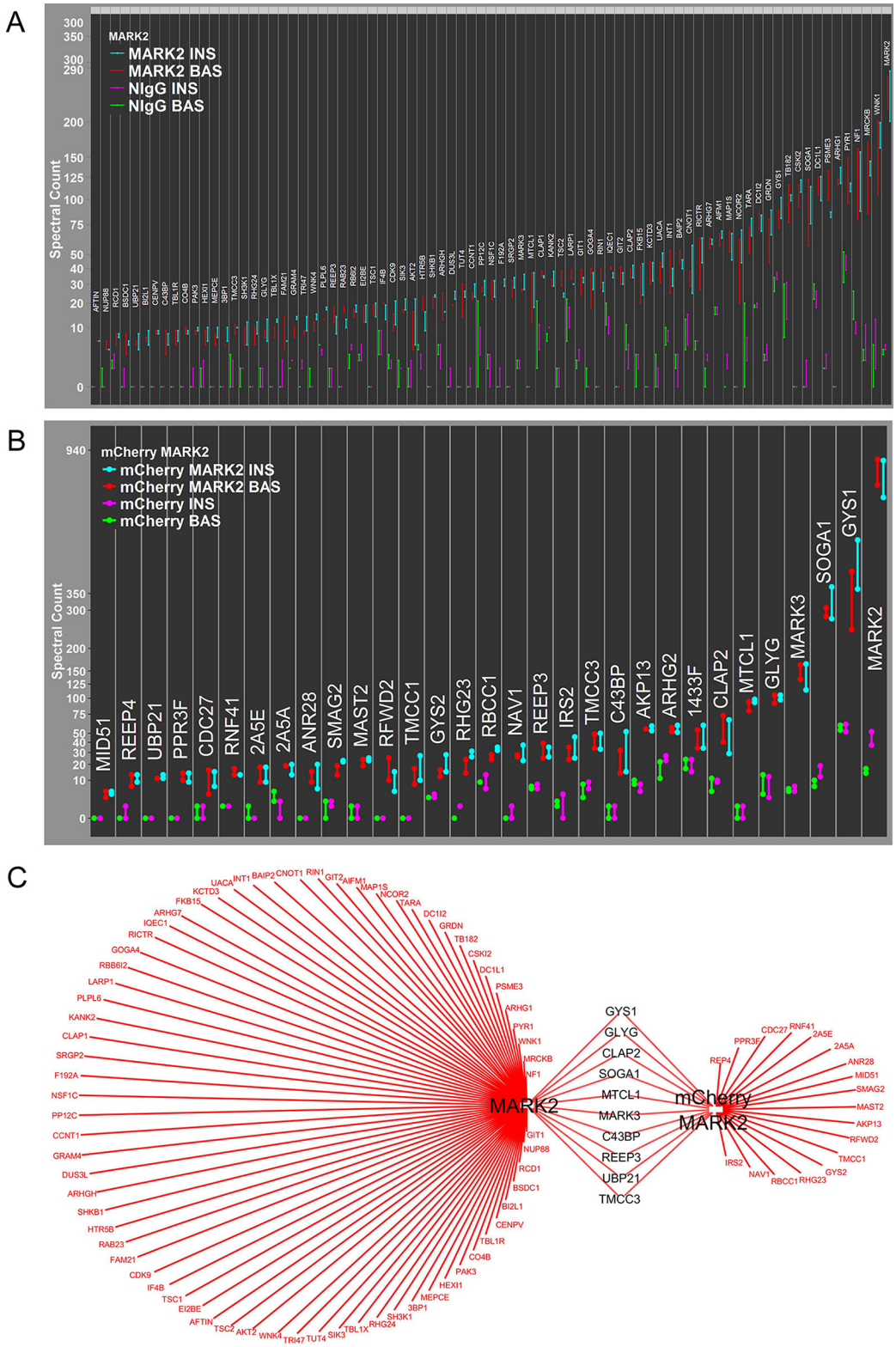

FIG. 5. **SCP analysis for the SAINT-qualified MARK2 and mCherry-MARK2 interactomes and Cytoscape-based MARK2/mCherry-MARK2 interactome integration.** *A*, MARK2 Antibody IPs and tandem mass spectrometry was performed as described under Experimental Procedures ($n = 2$) and SCP analysis of the 81 SAINT-qualified proteins is shown. *B*, Anti-mCherry Antibody IPs for mCherry-MARK2 and tandem mass spectrometry was performed as described under Experimental Procedures ($n = 2$) and SCP analysis of the 31 SAINT-qualified proteins is shown. *C*, Cytoscape-based integrated visual representation of the MARK2 and mCherry-MARK2 interactomes.

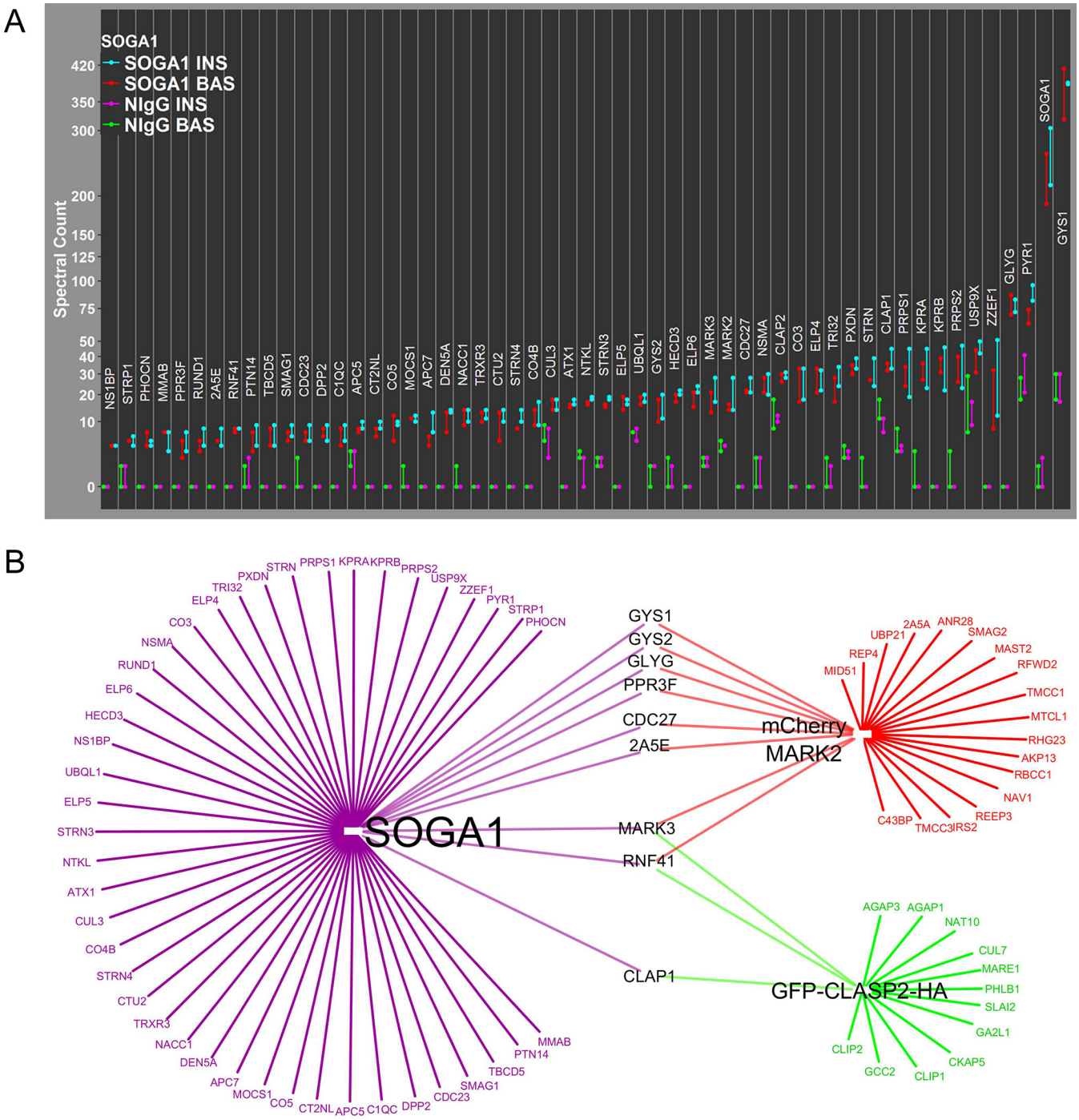

FIG. 6. **SCP analysis for the SAINT-qualified SOGA1 interactome and Cytoscape-based SOGA1/mCherry-MARK2/GFP-CLASP2-HA interactome integration.** *A*, Anti-SOGA1 Antibody IPs and tandem mass spectrometry was performed as described under Experimental Procedures ($n = 2$) and SCP analysis of the 55 SAINT-qualified proteins is shown. *B*, Cytoscape-based integrated visual representation of the SOGA1, mCherry-MARK2 and GFP-CLASP2-HA interactomes.

resulted in a best alignment/coverage score for the Cytoplasmic Dynein 2 Motor Domain (PDB ID 4RH7) (64). Using the dynein 2 domain as a template, the complete structure of SOGA1 was built *in silico*. Our analysis of the resulting structure indicates that SOGA1 shares a close similarity to the main features of dynein such as microtubule binding, stalk and strut domains (Fig. 9). SOGA1 sequence length is less than dynein 2, because of SOGA1 lacking the massive linker, neck, and tail portions of the dynein 2 N terminus. The SOGA1 structure predicts long N-terminal alpha-helixes of structural similarity to Tropomyosin chains, which could hypothetically interact with actin fibers after release from the observed "clamp"

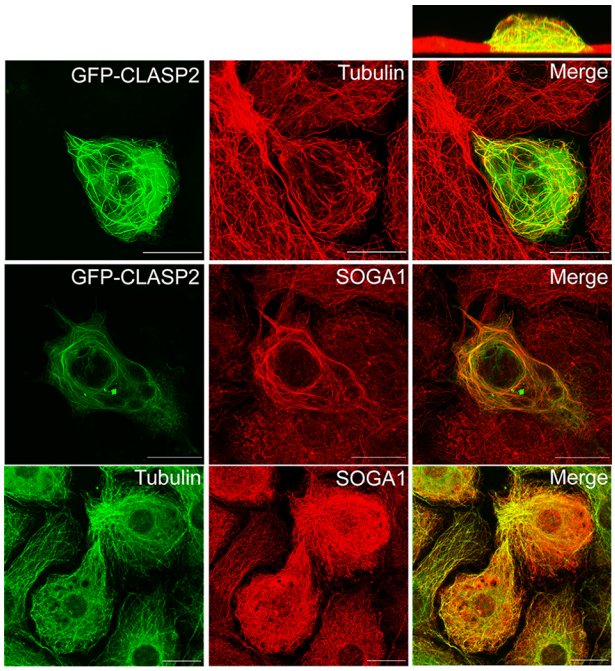

FIG. 7. **Identification of SOGA1 as a microtubule associated protein.** Adipocytes infected with GFP-CLASP2-HA adenovirus were imaged for GFP to visualize CLASP2 (top row, first panel) and immunostained for tubulin to visualize microtubules (top row, middle panel). These images were merged (top row, third panel) and a cross-sectional view of the z-plane is shown (above the third panel of the top row). Adipocytes infected with GFP-CLASP2-HA adenovirus were imaged for GFP to visualize CLASP2 (middle row, first panel) and immunostained for SOGA1 (middle row, middle panel). Adipocytes were immunostained for tubulin to visualize microtubules (bottom row, first panel) as well as SOGA1 (bottom row, second panel).

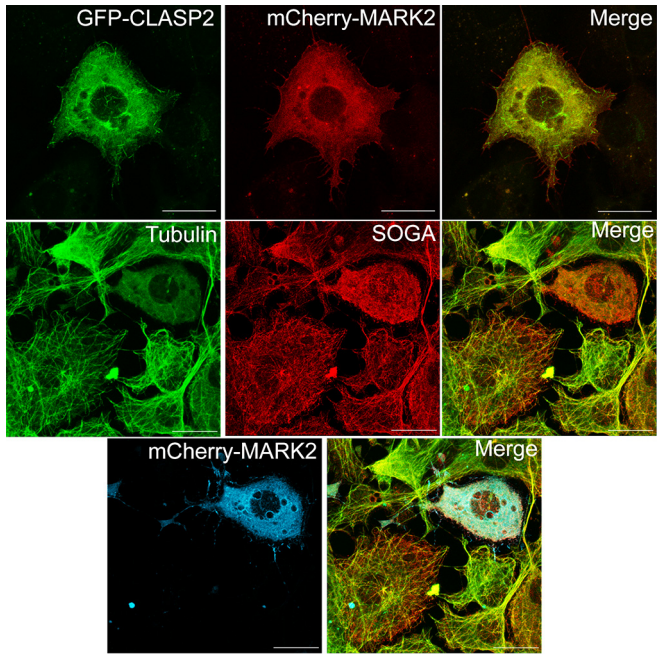

FIG. 8. **MARK2 overexpression disrupts CLASP2 and SOGA1 colocalization with microtubules.** Adipocytes infected with GFP-CLASP2-HA and mCherry-MARK2 adenovirus were imaged for GFP to visualize CLASP2 (top row, first panel) and mCherry to visualize MARK2 (top row, middle panel). Adipocytes infected with mCherry-MARK2 adenovirus were immunostained for tubulin to visualize microtubules (middle row, first panel) as well as SOGA1 (middle row, middle panel) and imaged for mCherry to visualize MARK2 (bottom row, first panel).

structure (Fig. 9, top right inset). Further structure-function experiments for SOGA1 will be the focus of future follow up studies. The molecular modeling data indicating SOGA1 is structurally like a known microtubule binding protein like dynein 2 is in agreement with the findings that SOGA1 colocalizes with CLASP2 and tubulin and supports the identification of SOGA1 as a new microtubule-associated protein.

DISCUSSION

We have developed and successfully executed a streamlined interactome approach to characterize the CLASP2 interactome in a 3T3-L1 adipocyte system. We compared NIgG antibody negative control IPs against two different CLASP2 antibody IPs and combined these interactomes with one null anti-HA antibody IP *versus* a GFP-CLASP2-HA anti-HA antibody IP and analyzed the raw interactome data with SAINT to identify proteins enriched in the CLASP2 IPs. To aid in the visualization of the raw spectral count data from the interactome experiments, we developed the Spectrum Count Profile, which allowed for facilitated interpretation of the raw spectral count results. By performing these in-depth, multiple antibody interactome experiments, we discovered that different antibodies for the same protein, in this case CLASP2 and MARK2, can present individually diverse interactomes, while also containing cross-correlating proteins as well. Taking this into account for the CLASP2 data, we narrowed down our focus to AGAP3 as one of the proteins of interest in the CLASP2 interactome. Subsequent analysis of the AGAP3 interactome revealed a strong enrichment of CLIP2 but not CLASP2, opening the likelihood that AGAP3 appeared in the CLASP2 interactome as a result of associating with CLIP2 (which was highly present in all three CLASP2 interactomes tested). In support of this, successive experiments performed to characterize the CLIP2 interactome revealed robust enrichment of AGAP3. AGAP3 coimmunoprecipitated AGAP1 very strongly, which may support the proposed functional cooperativity between AGAP family members (84), as AGAP1 and AGAP3 were also detected in tandem in the CLIP2 interactome and all three CLASP2 interactomes. The AGAPs, also referred to as the centaurins (85) and the GGAPs (86), have been shown to act as GAPs for Arf family members (79, 84) and have intrinsic GTPase property as well (85, 86), although GTPase activity has been questioned (79, 84). The fact that AGAP1 and AGAP3 consistently co-immunoprecipitated with the microtubule-associated proteins CLIP2 and CLASP2 now places these two proteins in position to be tested for roles in regulating microtubule dynamics. TBC1D4/AS160 is a GAP whose

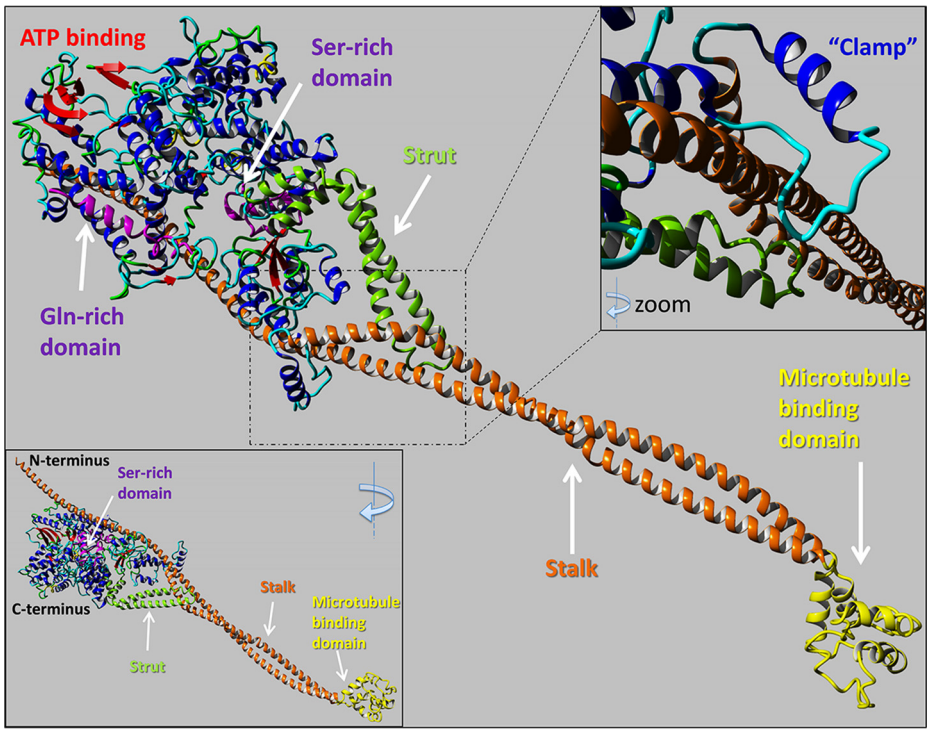

FIG. 9. **Homology model of SOGA1 structure.** Yasara molecular modeling software was used to build a homology model of SOGA1 structure. Homology modeling of the SOGA1 sequence results in a structure like dynein 2 (PDB ID 4RH7). The SOGA1 model has high similarity with structural characteristics of dynein 2 including a microtubule binding region (yellow) and both stalk (orange) and strut (green) domains. SOGA1 is predicted to contain only one ATP binding site (red), whereas dynein 2 posesses six distinctive ATP binding sites. SOGA1 contains both Serine- and Glutamine- rich sequences (purple) and a long N-terminal alpha-helix structure that has structural and sequence similarity to the actin binding protein tropomyosin. SOGA1 is predicted to contain a "clamp" region around the long N-terminal tropomyosin-like alpha-helix structure (the clamp feature is colored in blue within the top right inset).

inhibitory control of Rab function in GLUT4 translocation is deactivated by insulin-stimulated AKT phosphorylation (87). Based on our interactome findings, we hypothesize that both AGAP1 and AGAP3 are linked to CLASP2 through CLIP2, and because CLASP2 undergoes strong insulin-stimulated phosphorylation (16), it will be of interest to explore whether the proposed GTPase activity of the AGAP proteins is under the control of insulin-stimulated AGAP phosphorylation.

Another novel finding was that G2L1 (Uniprot gene name GAS2L1; protein name also known as GAR22) exhibited enrichment in all three CLASP2 interactomes as well as in the CLIP2 interactome. G2L1, like CLASP2, contains microtubule-tip localization sequences, which supports likely colocalization and possible cooperativity between these two proteins, and perhaps CLIP2 as well. G2L1 has been shown to bind with both filamentous actin (F-actin) and microtubules (88–91) to support microtubule and actin coalignment (88, 92). G2L1 mediates actin and microtubule crosstalk by promoting microtubule guidance along actin, which is of interest to insulin action because it has been proposed that the GSV could at some point transfer from microtubules to actin during the vesicle translocation process (93). This hypothesis is supported by the findings that knockdown of the actin-based motor proteins Myo1c and Myo5, which are responsible for cargo transport along actin, reduced cell surface levels of GLUT4 (94–96). It is also worth noting that both CLASP1 and CLASP2 have been found to interact with actin filaments (97). Future studies will investigate the functional consequences for the proposed CLASP2-CLIP2-G2L1 protein network, and the importance this complex has in regulating the function of these individual proteins.

With regards to the known associating partners for CLASP2, CLIP1, and CLIP2, both had excellent enrichment in the CLASP2 IPs, although there was no observable insulin effect on the co-IP of the two CLIPs with CLASP2 as tested, nor did insulin affect CLASP2 (or CLASP1) co-IP in the CLIP2 interactome. There has been a reported association between insulin action and the CLIP proteins, in that CLIP1 restores insulin-stimulated GLUT4 translocation in TSC2$^{-/-}$ cells, a mechanism postulated to involve mTOR-regulated microtubule organization (98) because mTOR can phosphorylate CLIP1 (99). CLIP2 and CLASP2 both shared association with CLIP1 and CLASP1, as well as with the binding partners SLAIN2 and CKAP5/ch-TOG, which is agreement with previous findings implicating that the microtubule plus end-tracking proteins SLAIN2, CKAP5, CLIP2, and CLASP2 can complex together (78). Another novel finding resulting from this study was the shared association of CLIP2 and AGAP3 with

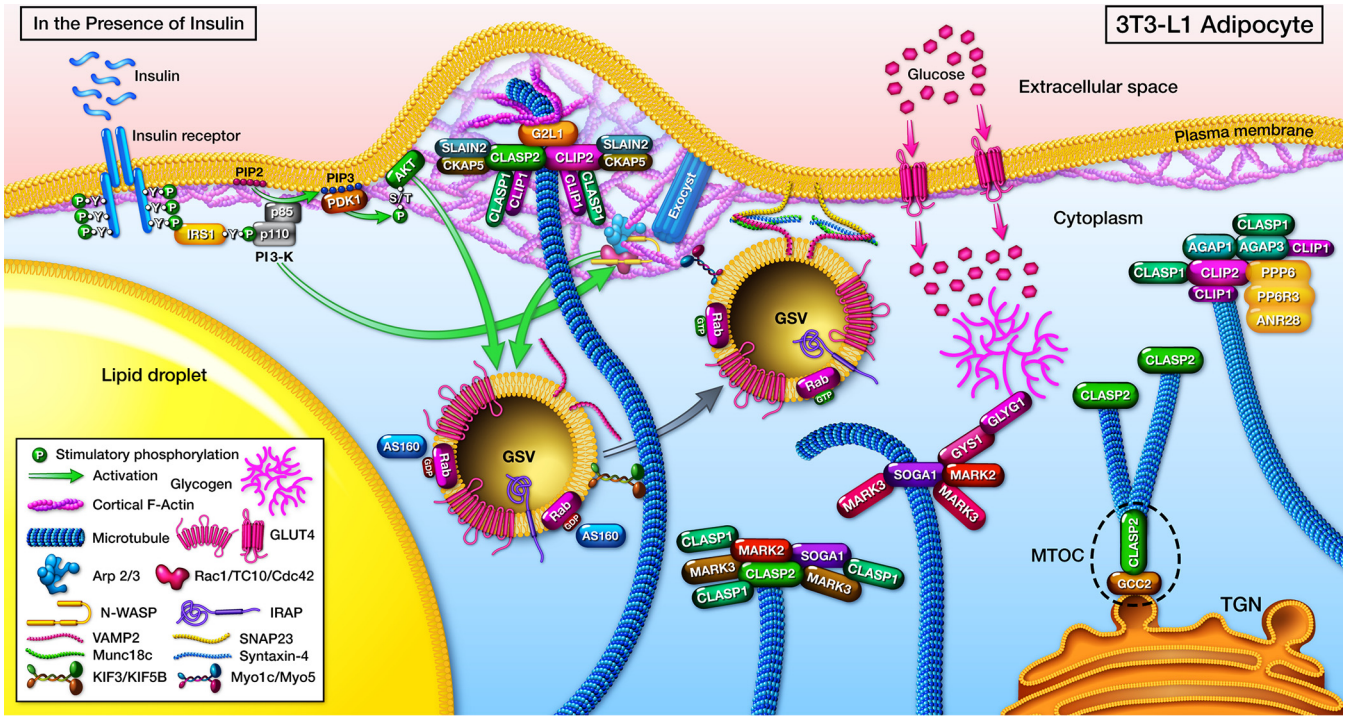

FIG. 10. **A hypothetical CLASP2 network model in 3T3-L1 adipocytes relative to insulin-stimulated glucose uptake.** From the interactome experiments conducted within 3T3-L1 adipocytes that we present in this study, we propose the hypothesis that CLASP2 proteins are partitioned out to various distinct complexes that are composed of both unique and shared proteins, and each complex possesses the likelihood of being functionally distinct. At the *trans*-Golgi network (TGN), CLASP2 has already been found to associate with GCC2/GCC185 and other proteins as part of a microtubule organization center (MTOC). At the plasma membrane, we propose the hypothesis that CLASP2, CLIP2 and G2L1 (possibly SLAIN2 and CKAP5 as well) and both CLASP1 and CLIP1 exist together to coordinate cytoskeletal events between the plus end of microtubules and perhaps insulin-stimulated cortically-reorganized actin. We also hypothesize that CLASP2 can associate with both MARK2 and SOGA1 in a separate complex, to coordinate dynamic stability of the microtubule. An alternative complex of MARK2/SOGA1, localized to microtubules, may functionally link glycogen synthase, glycogenin, and microtubules to glycogen management. The final complex revolves around the observed relationship between AGAP3 and CLIP2, which includes AGAP1, CLASP1, CLIP1 and members of the protein phosphatase 6 holoenzyme, specifically PPP6/PP6C, PP6R3, and ANR28. The hypothetical function of this complex may be to integrate the regulation of the dynamic instability of the plus end of the microtubule together with plus end-associated proteins and the GTPase activity of the AGAP1 and AGAP3 proteins.

ANR28, PP6R3 and PPP6, all of which are subunits of the serine/threonine-protein phosphatase 6 holoenzyme complex. Seeing as phosphorylation is a known modulator of GAP activity, the protein phosphatase 6 holoenzyme complex may contribute to the dynamic regulation of AGAP function.

We present the discovery that SOGA1, a protein with no previous connection to cytoskeletal elements, is enriched in the CLASP2 interactome. This finding was strengthened by successive analysis and confirmation of the presence of CLASP2 in the reciprocal SOGA1 interactome. SOGA1 is a relatively uncharacterized protein that has been linked to the regulation of autophagy in hepatocytes (82). In response to nutritional deprivation, autophagy can initiate the release of glucose from the liver by promoting the hydrolysis of proteins, glycogen, and triglycerides (100–102). SOGA1 expression was shown to be increased upon adiponectin-stimulated activation of the insulin signaling pathway in hepatocytes, and this increase in SOGA1 protein levels contributes to the reduction of glucose production by inhibiting autophagy through an as-of-yet unknown mechanism (82). These previous findings highlight the importance of our discovery that glycogen synthase (GYS1), the key biosynthetic enzyme for the synthesis of glycogen (103), is enriched in the SOGA1 interactome. Although the role of glycogen autophagy in adipocytes was only recently examined (104), it is possible to hypothesize that SOGA1 may regulate glucose and glycogen metabolism by directly cooperating with glycogen synthase and the glycogen synthase-associated protein glycogenin, which was also detected in the SOGA1 interactome. Because increased expression of SOGA1 was found to enhance inhibition of glycogen autophagy (82), SOGA1 binding to glycogen synthase and glycogenin could hypothetically participate in the protection of glycogen from autophagy, although these new proposed interactions from our proteomics studies will require further validation. In addition, this mechanism likely involves a microtubule element because SOGA1 subcellular localization studies presented here revealed SOGA1 as a new

microtubule-associated protein and molecular modeling studies predict SOGA1 to have a structure similar to the known microtubule binding protein dynein. This hypothesis is further strengthened by the additional discovery of MARK2 and MARK3 in the SOGA1 interactome, both of which are kinases known to regulate microtubule dynamics. Whereas CLASP2 promotes microtubule stability, MARK family members can disrupt microtubule growth (105), a phenomenon we showed that also results in the subcellular displacement of both SOGA1 and CLASP2 in adipocytes. The MARK family of protein kinases do have an established connection to metabolism, as MARK2, MARK3, and MARK4 knockout mice each exhibit enhanced peripheral insulin sensitivity and resistance to high-fat diet induced obesity (106–108). In addition, the MARK family of kinases are closely related to the energy sensor and metabolic regulator AMPK, as these kinases share a common consensus phosphorylation motif (109). These observations, together with the discovery presented here that MARK2, like SOGA1, can co-IP glycogen synthase and glycogenin, introduce the proposed SOGA1-MARK2-GYS1-GLYG network and microtubules as targets for studies aimed at determining the metabolic function of this potentially novel protein complex.

By taking advantage of proteomics and the advancements that are being made in interactome studies and bioinformatic resources, this study has made progress in identifying proteins that potentially associate with CLASP2, which has allowed us to propose a series of novel protein networks (Fig. 10). The discoveries presented here will lead to future studies aimed at further confirming these findings and understanding the purpose of the functional relationship these new protein networks have with microtubule dynamics, actin reorganization, glucose and glycogen metabolism, autophagy, and insulin action.

Acknowledgments—We thank Marv Ruona for his artistic renderings included in this article.

DATA AVAILABILITY

The .RAW files and Scaffold data (in mzIdent format) for all experiments have been deposited to the ProteomeXchange Consortium (http://proteomecentral.proteomexchange.org) via the PRIDE partner repository with the data set identifier: PXD003674.

* The content is solely the responsibility of the authors and does not necessarily represent the official views of the National Institutes of Health.

[S] This article contains supplemental material.

** To whom correspondence should be addressed: Department of Medicine, Division of Endocrinology, University of Arizona College of Medicine, 1501 N. Campbell Ave, Tucson, AZ 85721. Tel.: 520-626-1342; E-mail: langlais@deptofmed.arizona.edu.

REFERENCES

1. Khayat, Z. A., Tong, P., Yaworsky, K., Bloch, R. J., and Klip, A. (2000) Insulin-induced actin filament remodeling colocalizes actin with phosphatidylinositol 3-kinase and GLUT4 in L6 myotubes. *J. Cell Sci.* **113 Pt 2,** 279–290
2. Patel, N., Rudich, A., Khayat, Z. A., Garg, R., and Klip, A. (2003) Intracellular segregation of phosphatidylinositol-3,4,5-trisphosphate by insulin-dependent actin remodeling in L6 skeletal muscle cells. *Mol. Cell. Biol.* **23,** 4611–4626
3. Zaid, H., Antonescu, C. N., Randhawa, V. K., and Klip, A. (2008) Insulin action on glucose transporters through molecular switches, tracks and tethers. *Biochem. J.* **413,** 201–215
4. Kanzaki, M., and Pessin, J. E. (2001) Insulin-stimulated GLUT4 translocation in adipocytes is dependent upon cortical actin remodeling. *J. Biol. Chem.* **276,** 42436–42444
5. Wang, Q., Bilan, P. J., Tsakiridis, T., Hinek, A., and Klip, A. (1998) Actin filaments participate in the relocalization of phosphatidylinositol3-kinase to glucose transporter-containing compartments and in the stimulation of glucose uptake in 3T3-L1 adipocytes. *Biochem. J.* **331 (Pt 3),** 917–928
6. Tong, P., Khayat, Z. A., Huang, C., Patel, N., Ueyama, A., and Klip, A. (2001) Insulin-induced cortical actin remodeling promotes GLUT4 insertion at muscle cell membrane ruffles. *J. Clin. Invest.* **108,** 371–381
7. Omata, W., Shibata, H., Li, L., Takata, K., and Kojima, I. (2000) Actin filaments play a critical role in insulin-induced exocytotic recruitment but not in endocytosis of GLUT4 in isolated rat adipocytes. *Biochem. J.* **346 Pt 2,** 321–328
8. Brozinick, J. T., Jr, Hawkins, E. D., Strawbridge, A. B., and Elmendorf, J. S. (2004) Disruption of cortical actin in skeletal muscle demonstrates an essential role of the cytoskeleton in glucose transporter 4 translocation in insulin-sensitive tissues. *J. Biol. Chem.* **279,** 40699–40706
9. Desai, A., and Mitchison, T. J. (1997) Microtubule polymerization dynamics. *Annu. Rev. Cell Dev. Biol.* **13,** 83–117
10. Dawicki-McKenna, J. M., Goldman, Y. E., and Ostap, E. M. (2012) Sites of glucose transporter-4 vesicle fusion with the plasma membrane correlate spatially with microtubules. *PLoS ONE* **7,** e43662
11. Xu, Y. K., Xu, K. D., Li, J. Y., Feng, L. Q., Lang, D., and Zheng, X. X. (2007) Bi-directional transport of GLUT4 vesicles near the plasma membrane of primary rat adipocytes. *Biochem. Biophys. Res. Commun.* **359,** 121–128
12. Chen, Y., Wang, Y., Ji, W., Xu, P., and Xu, T. (2008) A pre-docking role for microtubules in insulin-stimulated glucose transporter 4 translocation. *FEBS J.* **275,** 705–712
13. Emoto, M., Langille, S. E., and Czech, M. P. (2001) A role for kinesin in insulin-stimulated GLUT4 glucose transporter translocation in 3T3-L1 adipocytes. *J. Biol. Chem.* **276,** 10677–10682
14. Semiz, S., Park, J. G., Nicoloro, S. M., Furcinitti, P., Zhang, C., Chawla, A., Leszyk, J., and Czech, M. P. (2003) Conventional kinesin KIF5B mediates insulin-stimulated GLUT4 movements on microtubules. *EMBO J.* **22,** 2387–2399
15. Imamura, T., Huang, J., Usui, I., Satoh, H., Bever, J., and Olefsky, J. M. (2003) Insulin-induced GLUT4 translocation involves protein kinase C-lambda-mediated functional coupling between Rab4 and the motor protein kinesin. *Mol. Cell. Biol.* **23,** 4892–4900
16. Langlais, P., Dillon, J. L., Mengos, A., Baluch, D. P., Ardebili, R., Miranda, D. N., Xie, X., Heckmann, B. L., Liu, J., and Mandarino, L. J. (2012) Identification of a role for CLASP2 in insulin action. *J. Biol. Chem.* **287,** 39245–39253
17. Akhmanova, A., Hoogenraad, C. C., Drabek, K., Stepanova, T., Dortland, B., Verkerk, T., Vermeulen, W., Burgering, B. M., De Zeeuw, C. I., Grosveld, F., and Galjart, N. (2001) Clasps are CLIP-115 and -170 associating proteins involved in the regional regulation of microtubule dynamics in motile fibroblasts. *Cell* **104,** 923–935
18. Maiato, H., Fairley, E. A., Rieder, C. L., Swedlow, J. R., Sunkel, C. E., and Earnshaw, W. C. (2003) Human CLASP1 is an outer kinetochore component that regulates spindle microtubule dynamics. *Cell* **113,** 891–904
19. Moore, C. A., and Zernicka-Goetz, M. (2005) PAR-1 and the microtubule-associated proteins CLASP2 and dynactin-p50 have specific localisation on mouse meiotic and first mitotic spindles. *Reproduction* **130,** 311–320
20. Pereira, A. L., Pereira, A. J., Maia, A. R., Drabek, K., Sayas, C. L., Hergert, P. J., Lince-Faria, M., Matos, I., Duque, C., Stepanova, T., Rieder, C. L., Earnshaw, W. C., Galjart, N., and Maiato, H. (2006) Mammalian CLASP1

and CLASP2 cooperate to ensure mitotic fidelity by regulating spindle and kinetochore function. *Mol. Biol. Cell* **17,** 4526–4542
21. Maffini, S., Maia, A. R., Manning, A. L., Maliga, Z., Pereira, A. L., Junqueira, M., Shevchenko, A., Hyman, A., Yates, J. R., 3rd, Galjart, N., Compton, D. A., and Maiato, H. (2009) Motor-independent targeting of CLASPs to kinetochores by CENP-E promotes microtubule turnover and poleward flux. *Curr. Biol.* **19,** 1566–1572
22. Manning, A. L., Bakhoum, S. F., Maffini, S., Correia-Melo, C., Maiato, H., and Compton, D. A. (2010) CLASP1, astrin and Kif2b form a molecular switch that regulates kinetochore-microtubule dynamics to promote mitotic progression and fidelity. *EMBO J.* **29,** 3531–3543
23. Maia, A. R., Garcia, Z., Kabeche, L., Barisic, M., Maffini, S., Macedo-Ribeiro, S., Cheeseman, I. M., Compton, D. A., Kaverina, I., and Maiato, H. (2012) Cdk1 and Plk1 mediate a CLASP2 phospho-switch that stabilizes kinetochore-microtubule attachments. *J. Cell Biol.* **199,** 285–301
24. Mimori-Kiyosue, Y., Grigoriev, I., Lansbergen, G., Sasaki, H., Matsui, C., Severin, F., Galjart, N., Grosveld, F., Vorobjev, I., Tsukita, S., and Akhmanova, A. (2005) CLASP1 and CLASP2 bind to EB1 and regulate microtubule plus-end dynamics at the cell cortex. *J. Cell Biol.* **168,** 141–153
25. Lansbergen, G., Grigoriev, I., Mimori-Kiyosue, Y., Ohtsuka, T., Higa, S., Kitajima, I., Demmers, J., Galjart, N., Houtsmuller, A. B., Grosveld, F., and Akhmanova, A. (2006) CLASPs attach microtubule plus ends to the cell cortex through a complex with LL5beta. *Dev. Cell* **11,** 21–32
26. Nakamura, S., Grigoriev, I., Nogi, T., Hamaji, T., Cassimeris, L., and Mimori-Kiyosue, Y. (2012) Dissecting the nanoscale distributions and functions of microtubule-end-binding proteins EB1 and ch-TOG in interphase HeLa cells. *PLoS ONE* **7,** e51442
27. Ruiz-Saenz, A., van Haren, J., Laura Sayas, C., Rangel, L., Demmers, J., Millan, J., Alonso, M. A., Galjart, N., and Correas, I. (2013) Protein 4.1R binds to CLASP2 and regulates dynamics, organization and attachment of microtubules to the cell cortex. *J. Cell Sci.* **126,** 4589–4601
28. Wittmann, T., and Waterman-Storer, C. M. (2005) Spatial regulation of CLASP affinity for microtubules by Rac1 and GSK3beta in migrating epithelial cells. *J. Cell Biol.* **169,** 929–939
29. Kumar, P., Lyle, K. S., Gierke, S., Matov, A., Danuser, G., and Wittmann, T. (2009) GSK3beta phosphorylation modulates CLASP-microtubule association and lamella microtubule attachment. *J. Cell Biol.* **184,** 895–908
30. Watanabe, T., Noritake, J., Kakeno, M., Matsui, T., Harada, T., Wang, S., Itoh, N., Sato, K., Matsuzawa, K., Iwamatsu, A., Galjart, N., and Kaibuchi, K. (2009) Phosphorylation of CLASP2 by GSK-3beta regulates its interaction with IQGAP1, EB1 and microtubules. *J. Cell Sci.* **122,** 2969–2979
31. Logue, J. S., Whiting, J. L., Tunquist, B., Sacks, D. B., Langeberg, L. K., Wordeman, L., and Scott, J. D. (2011) AKAP220 protein organizes signaling elements that impact cell migration. *J. Biol. Chem.* **286,** 39269–39281
32. Efimov, A., Kharitonov, A., Efimova, N., Loncarek, J., Miller, P. M., Andreyeva, N., Gleeson, P., Galjart, N., Maia, A. R., McLeod, I. X., Yates, J. R., 3rd, Maiato, H., Khodjakov, A., Akhmanova, A., and Kaverina, I. (2007) Asymmetric CLASP-dependent nucleation of noncentrosomal microtubules at the trans-Golgi network. *Dev. Cell* **12,** 917–930
33. Miller, P. M., Folkmann, A. W., Maia, A. R., Efimova, N., Efimov, A., and Kaverina, I. (2009) Golgi-derived CLASP-dependent microtubules control Golgi organization and polarized trafficking in motile cells. *Nat. Cell Biol.* **11,** 1069–1080
34. Rivero, S., Cardenas, J., Bornens, M., and Rios, R. M. (2009) Microtubule nucleation at the cis-side of the Golgi apparatus requires AKAP450 and GM130. *EMBO J.* **28,** 1016–1028
35. Adachi, A., Kano, F., Tsuboi, T., Fujita, M., Maeda, Y., and Murata, M. (2010) Golgi-associated GSK3beta regulates the sorting process of post-Golgi membrane trafficking. *J. Cell Sci.* **123,** 3215–3225
36. Lin, Y. C., Chiang, T. C., Liu, Y. T., Tsai, Y. T., Jang, L. T., and Lee, F. J. (2011) ARL4A acts with GCC185 to modulate Golgi complex organization. *J. Cell Sci.* **124,** 4014–4026
37. Sato, Y., Hayashi, K., Amano, Y., Takahashi, M., Yonemura, S., Hayashi, I., Hirose, H., Ohno, S., and Suzuki, A. (2014) MTCL1 crosslinks and stabilizes noncentrosomal microtubules on the Golgi membrane. *Nat. Commun.* **5,** 5266
38. Matsui, T., Watanabe, T., Matsuzawa, K., Kakeno, M., Okumura, N., Sugiyama, I., Itoh, N., and Kaibuchi, K. (2015) PAR3 and aPKC regulate Golgi organization through CLASP2 phosphorylation to generate cell polarity. *Mol. Biol. Cell* **26,** 751–761
39. Hur, E. M., Saijilafu Lee, B. D., Kim, S. J., Xu, W. L., and Zhou, F. Q. (2011) GSK3 controls axon growth via CLASP-mediated regulation of growth cone microtubules. *Genes Dev.* **25,** 1968–1981
40. Beffert, U., Dillon, G. M., Sullivan, J. M., Stuart, C. E., Gilbert, J. P., Kambouris, J. A., and Ho, A. (2012) Microtubule plus-end tracking protein CLASP2 regulates neuronal polarity and synaptic function. *J. Neurosci.* **32,** 13906–13916
41. Kim, D. J., Martinez-Lemus, L. A., and Davis, G. E. (2013) EB1, p150Glued, and Clasp1 control endothelial tubulogenesis through microtubule assembly, acetylation, and apical polarization. *Blood* **121,** 3521–3530
42. Shahbazi, M. N., Megias, D., Epifano, C., Akhmanova, A., Gundersen, G. G., Fuchs, E., and Perez-Moreno, M. (2013) CLASP2 interacts with p120-catenin and governs microtubule dynamics at adherens junctions. *J. Cell Biol.* **203,** 1043–1061
43. Shahbazi, M. N., and Perez-Moreno, M. (2014) Microtubules CLASP to Adherens Junctions in epidermal progenitor cells. *Bioarchitecture* **4,** 25–30
44. Basu, S., Sladecek, S., Pemble, H., Wittmann, T., Slotman, J. A., van Cappellen, W., Brenner, H. R., and Galjart, N. (2014) Acetylcholine receptor (AChR) clustering is regulated both by glycogen synthase kinase 3beta (GSK3beta)-dependent phosphorylation and the level of CLIP-associated protein 2 (CLASP2) mediating the capture of microtubule plus-ends. *J. Biol. Chem.* **289,** 30857–30867
45. Schmidt, N., Basu, S., Sladecek, S., Gatti, S., van Haren, J., Treves, S., Pielage, J., Galjart, N., and Brenner, H. R. (2012) Agrin regulates CLASP2-mediated capture of microtubules at the neuromuscular junction synaptic membrane. *J. Cell Biol.* **198,** 421–437
46. Basu, S., Sladecek, S., Martinez de la Pena y Valenzuela, I., Akaaboune, M., Smal, I., Martin, K., Galjart, N., and Brenner, H. R. (2015) CLASP2-dependent microtubule capture at the neuromuscular junction membrane requires LL5beta and actin for focal delivery of acetylcholine receptor vesicles. *Mol. Biol. Cell* **26,** 938–951
47. Efimova, N., Grimaldi, A., Bachmann, A., Frye, K., Zhu, X., Feoktistov, A., Straube, A., and Kaverina, I. (2014) Podosome-regulating kinesin KIF1C translocates to the cell periphery in a CLASP-dependent manner. *J. Cell Sci.* **127,** 5179–5188
48. Stehbens, S. J., Paszek, M., Pemble, H., Ettinger, A., Gierke, S., and Wittmann, T. (2014) CLASPs link focal-adhesion-associated microtubule capture to localized exocytosis and adhesion site turnover. *Nat. Cell Biol.* **16,** 561–573
49. Galjart, N. (2005) CLIPs and CLASPs and cellular dynamics. *Nat. Rev. Mol. Cell Biol.* **6,** 487–498
50. Akhmanova, A., and Steinmetz, M. O. (2008) Tracking the ends: a dynamic protein network controls the fate of microtubule tips. *Nat. Rev. Mol. Cell Biol.* **9,** 309–322
51. Galjart, N. (2010) Plus-end-tracking proteins and their interactions at microtubule ends. *Curr. Biol.* **20,** R528–R537
52. Al-Bassam, J., and Chang, F. (2011) Regulation of microtubule dynamics by TOG-domain proteins XMAP215/Dis1 and CLASP. *Trends Cell Biol.* **21,** 604–614
53. Tamura, N., and Draviam, V. M. (2012) Microtubule plus-ends within a mitotic cell are 'moving platforms' with anchoring, signalling and force-coupling roles. *Open Biol.* **2,** 120132
54. Duellberg, C., Fourniol, F. J., Maurer, S. P., Roostalu, J., and Surrey, T. (2013) End-binding proteins and Ase1/PRC1 define local functionality of structurally distinct parts of the microtubule cytoskeleton. *Trends Cell Biol.* **23,** 54–63
55. Rios, R. M. (2014) The centrosome-Golgi apparatus nexus. *Philos. Trans. R. Soc. Lond. B Biol. Sci.* **369**
56. Zhou, Q. L., Jiang, Z. Y., Mabardy, A. S., Del Campo, C. M., Lambright, D. G., Holik, J., Fogarty, K. E., Straubhaar, J., Nicoloro, S., Chawla, A., and Czech, M. P. (2010) A novel pleckstrin homology domain-containing protein enhances insulin-stimulated Akt phosphorylation and GLUT4 translocation in adipocytes. *J. Biol. Chem.* **285,** 27581–27589
57. Markan, K. R., Jurczak, M. J., Allison, M. B., Ye, H., Sutanto, M. M., Cohen, R. N., and Brady, M. J. (2010) Enhanced glycogen metabolism

in adipose tissue decreases triglyceride mobilization. *Am. J. Physiol. Endocrinol. Metab.* **299,** E117–E125
58. Choi, H., Larsen, B., Lin, Z. Y., Breitkreutz, A., Mellacheruvu, D., Fermin, D., Qin, Z. S., Tyers, M., Gingras, A. C., and Nesvizhskii, A. I. (2011) SAINT: probabilistic scoring of affinity purification-mass spectrometry data. *Nat. Methods* **8,** 70–73
59. Choi, H., Glatter, T., Gstaiger, M., and Nesvizhskii, A. I. (2012) SAINT-MS1: protein-protein interaction scoring using label-free intensity data in affinity purification-mass spectrometry experiments. *J. Proteome Res.* **11,** 2619–2624
60. Choi, H., Liu, G., Mellacheruvu, D., Tyers, M., Gingras, A. C., and Nesvizhskii, A. I. (2012) Analyzing protein-protein interactions from affinity purification-mass spectrometry data with SAINT. *Curr. Protoc. Bioinformatics* **Chapter 8,** Unit8 15
61. Teo, G., Liu, G., Zhang, J., Nesvizhskii, A. I., Gingras, A. C., and Choi, H. (2014) SAINTexpress: improvements and additional features in Significance Analysis of INTeractome software. *J. Proteomics* **100,** 37–43
62. Chambers, M. C., Maclean, B., Burke, R., Amodei, D., Ruderman, D. L., Neumann, S., Gatto, L., Fischer, B., Pratt, B., Egertson, J., Hoff, K., Kessner, D., Tasman, N., Shulman, N., Frewen, B., Baker, T. A., Brusniak, M. Y., Paulse, C., Creasy, D., Flashner, L., Kani, K., Moulding, C., Seymour, S. L., Nuwaysir, L. M., Lefebvre, B., Kuhlmann, F., Roark, J., Rainer, P., Detlev, S., Hemenway, T., Huhmer, A., Langridge, J., Connolly, B., Chadick, T., Holly, K., Eckels, J., Deutsch, E. W., Moritz, R. L., Katz, J. E., Agus, D. B., MacCoss, M., Tabb, D. L., and Mallick, P. (2012) A cross-platform toolkit for mass spectrometry and proteomics. *Nat. Biotechnol.* **30,** 918–920
63. Vizcaino, J. A., Cote, R. G., Csordas, A., Dianes, J. A., Fabregat, A., Foster, J. M., Griss, J., Alpi, E., Birim, M., Contell, J., O'Kelly, G., Schoenegger, A., Ovelleiro, D., Perez-Riverol, Y., Reisinger, F., Rios, D., Wang, R., and Hermjakob, H. (2013) The PRoteomics IDEntifications (PRIDE) database and associated tools: status in 2013. *Nucleic Acids Res.* **41,** D1063–D1069
64. Schmidt, H., Zalyte, R., Urnavicius, L., and Carter, A. P. (2015) Structure of human cytoplasmic dynein-2 primed for its power stroke. *Nature* **518,** 435–438
65. Dunham, W. H., Mullin, M., and Gingras, A. C. (2012) Affinity-purification coupled to mass spectrometry: basic principles and strategies. *Proteomics* **12,** 1576–1590
66. Morris, J. H., Knudsen, G. M., Verschueren, E., Johnson, J. R., Cimermancic, P., Greninger, A. L., and Pico, A. R. (2014) Affinity purification-mass spectrometry and network analysis to understand protein-protein interactions. *Nat. Protoc.* **9,** 2539–2554
67. Westermarck, J., Ivaska, J., and Corthals, G. L. (2013) Identification of protein interactions involved in cellular signaling. *Mol. Cell. Proteomics* **12,** 1752–1763
68. Bedard, L. G., Dronamraju, R., Kerschner, J. L., Hunter, G. O., Axley, E. D., Boyd, A. K., Strahl, B. D., and Mosley, A. L. (2016) Quantitative Analysis of Dynamic Protein Interactions during Transcription Reveals a Role for Casein Kinase II in Polymerase-associated Factor (PAF) Complex Phosphorylation and Regulation of Histone H2B Monoubiquitylation. *J. Biol. Chem.* **291,** 13410–13420
69. Federspiel, J. D., Codreanu, S. G., Palubinsky, A. M., Winland, A. J., Betanzos, C. M., McLaughlin, B., and Liebler, D. C. (2016) Assembly Dynamics and Stoichiometry of the Apoptosis Signal-regulating Kinase (ASK) Signalosome in Response to Electrophile Stress. *Mol. Cell. Proteomics* **15,** 1947–1961
70. Huang, H., Alvarez, S., Bindbeutel, R., Shen, Z., Naldrett, M. J., Evans, B. S., Briggs, S. P., Hicks, L. M., Kay, S. A., and Nusinow, D. A. (2016) Identification of Evening Complex Associated Proteins in Arabidopsis by Affinity Purification and Mass Spectrometry. *Mol. Cell. Proteomics* **15,** 201–217
71. Merkulova, M., Paunescu, T. G., Azroyan, A., Marshansky, V., Breton, S., and Brown, D. (2015) Mapping the H(+) (V)-ATPase interactome: identification of proteins involved in trafficking, folding, assembly and phosphorylation. *Sci. Rep.* **5,** 14827
72. Scifo, E., Szwajda, A., Soliymani, R., Pezzini, F., Bianchi, M., Dapkunas, A., Debski, J., Uusi-Rauva, K., Dadlez, M., Gingras, A. C., Tyynela, J., Simonati, A., Jalanko, A., Baumann, M. H., and Lalowski, M. (2015) Quantitative analysis of PPT1 interactome in human neuroblastoma cells. *Data Brief* **4,** 207–216
73. Paul, V. D., Muhlenhoff, U., Stumpfig, M., Seebacher, J., Kugler, K. G., Renicke, C., Taxis, C., Gavin, A. C., Pierik, A. J., and Lill, R. (2015) The deca-GX3 proteins Yae1-Lto1 function as adaptors recruiting the ABC protein Rli1 for iron-sulfur cluster insertion. *Elife* **4,** e08231
74. Kumar, P., and Wittmann, T. (2012) +TIPs: SxIPping along microtubule ends. *Trends Cell Biol.* **22,** 418–428
75. Bogan, J. S., Hendon, N., McKee, A. E., Tsao, T. S., and Lodish, H. F. (2003) Functional cloning of TUG as a regulator of GLUT4 glucose transporter trafficking. *Nature* **425,** 727–733
76. Bogan, J. S., Rubin, B. R., Yu, C., Loffler, M. G., Orme, C. M., Belman, J. P., McNally, L. J., Hao, M., and Cresswell, J. A. (2012) Endoproteolytic cleavage of TUG protein regulates GLUT4 glucose transporter translocation. *J. Biol. Chem.* **287,** 23932–23947
77. Shannon, P., Markiel, A., Ozier, O., Baliga, N. S., Wang, J. T., Ramage, D., Amin, N., Schwikowski, B., and Ideker, T. (2003) Cytoscape: a software environment for integrated models of biomolecular interaction networks. *Genome Res.* **13,** 2498–2504
78. van der Vaart, B., Manatschal, C., Grigoriev, I., Olieric, V., Gouveia, S. M., Bjelic, S., Demmers, J., Vorobjev, I., Hoogenraad, C. C., Steinmetz, M. O., and Akhmanova, A. (2011) SLAIN2 links microtubule plus end-tracking proteins and controls microtubule growth in interphase. *J. Cell Biol.* **193,** 1083–1099
79. Nie, Z., Stanley, K. T., Stauffer, S., Jacques, K. M., Hirsch, D. S., Takei, J., and Randazzo, P. A. (2002) AGAP1, an endosome-associated, phosphoinositide-dependent ADP-ribosylation factor GTPase-activating protein that affects actin cytoskeleton. *J. Biol. Chem.* **277,** 48965–48975
80. Drewes, G., Ebneth, A., Preuss, U., Mandelkow, E. M., and Mandelkow, E. (1997) MARK, a novel family of protein kinases that phosphorylate microtubule-associated proteins and trigger microtubule disruption. *Cell* **89,** 297–308
81. Sato, Y., Akitsu, M., Amano, Y., Yamashita, K., Ide, M., Shimada, K., Yamashita, A., Hirano, H., Arakawa, N., Maki, T., Hayashi, I., Ohno, S., and Suzuki, A. (2013) The novel PAR-1-binding protein MTCL1 has crucial roles in organizing microtubules in polarizing epithelial cells. *J. Cell Sci.* **126,** 4671–4683
82. Cowherd, R. B., Asmar, M. M., Alderman, J. M., Alderman, E. A., Garland, A. L., Busby, W. H., Bodnar, W. M., Rusyn, I., Medoff, B. D., Tisch, R., Mayer-Davis, E., Swenberg, J. A., Zeisel, S. H., and Combs, T. P. (2010) Adiponectin lowers glucose production by increasing SOGA. *Am. J. Pathol.* **177,** 1936–1945
83. Krieger, E., Nabuurs, S. B., and Vriend, G. (2003) Homology modeling. *Methods Biochem. Anal.* **44,** 509–523
84. Luo, R., Akpan, I. O., Hayashi, R., Sramko, M., Barr, V., Shiba, Y., and Randazzo, P. A. (2012) GTP-binding protein-like domain of AGAP1 is protein binding site that allosterically regulates ArfGAP protein catalytic activity. *J. Biol. Chem.* **287,** 17176–17185
85. Soundararajan, M., Yang, X., Elkins, J. M., Sobott, F., and Doyle, D. A. (2007) The centaurin gamma-1 GTPase-like domain functions as an NTPase. *Biochem. J.* **401,** 679–688
86. Xia, C., Ma, W., Stafford, L. J., Liu, C., Gong, L., Martin, J. F., and Liu, M. (2003) GGAPs, a new family of bifunctional GTP-binding and GTPase-activating proteins. *Mol. Cell. Biol.* **23,** 2476–2488
87. Sano, H., Kane, S., Sano, E., Miinea, C. P., Asara, J. M., Lane, W. S., Garner, C. W., and Lienhard, G. E. (2003) Insulin-stimulated phosphorylation of a Rab GTPase-activating protein regulates GLUT4 translocation. *J. Biol. Chem.* **278,** 14599–14602
88. Stroud, M. J., Nazgiewicz, A., McKenzie, E. A., Wang, Y., Kammerer, R. A., and Ballestrem, C. (2014) GAS2-like proteins mediate communication between microtubules and actin through interactions with end-binding proteins. *J. Cell Sci.* **127,** 2672–2682
89. Goriounov, D., Leung, C. L., and Liem, R. K. (2003) Protein products of human Gas2-related genes on chromosomes 17 and 22 (hGAR17 and hGAR22) associate with both microfilaments and microtubules. *J. Cell Sci.* **116,** 1045–1058
90. Gamper, I., Koh, K. R., Ruau, D., Ullrich, K., Bartunkova, J., Piroth, D., Hacker, C., Bartunek, P., and Zenke, M. (2009) GAR22: a novel target gene of thyroid hormone receptor causes growth inhibition in human erythroid cells. *Exp. Hematol.* **37**, 539–548 e534
91. Gamper, I., Fleck, D., Barlin, M., Spehr, M., El Sayad, S., Kleine, H., Maxeiner, S., Schalla, C., Aydin, G., Hoss, M., Litchfield, D. W.,

Luscher, B., Zenke, M., and Sechi, A. (2016) GAR22beta regulates cell migration, sperm motility, and axoneme structure. *Mol. Biol. Cell* **27,** 277–294

92. Jiang, K., Toedt, G., Montenegro Gouveia, S., Davey, N. E., Hua, S., van der Vaart, B., Grigoriev, I., Larsen, J., Pedersen, L. B., Bezstarosti, K., Lince-Faria, M., Demmers, J., Steinmetz, M. O., Gibson, T. J., and Akhmanova, A. (2012) A Proteome-wide screen for mammalian SxIP motif-containing microtubule plus-end tracking proteins. *Curr. Biol.* **22,** 1800–1807
93. Talior-Volodarsky, I., Randhawa, V. K., Zaid, H., and Klip, A. (2008) Alpha-actinin-4 is selectively required for insulin-induced GLUT4 translocation. *J. Biol. Chem.* **283,** 25115–25123
94. Bose, A., Robida, S., Furcinitti, P. S., Chawla, A., Fogarty, K., Corvera, S., and Czech, M. P. (2004) Unconventional myosin Myo1c promotes membrane fusion in a regulated exocytic pathway. *Mol. Cell. Biol.* **24,** 5447–5458
95. Yoshizaki, T., Imamura, T., Babendure, J. L., Lu, J. C., Sonoda, N., and Olefsky, J. M. (2007) Myosin 5a is an insulin-stimulated Akt2 (protein kinase Bbeta) substrate modulating GLUT4 vesicle translocation. *Mol. Cell. Biol.* **27,** 5172–5183
96. Yip, M. F., Ramm, G., Larance, M., Hoehn, K. L., Wagner, M. C., Guilhaus, M., and James, D. E. (2008) CaMKII-mediated phosphorylation of the myosin motor Myo1c is required for insulin-stimulated GLUT4 translocation in adipocytes. *Cell Metab.* **8,** 384–398
97. Tsvetkov, A. S., Samsonov, A., Akhmanova, A., Galjart, N., and Popov, S. V. (2007) Microtubule-binding proteins CLASP1 and CLASP2 interact with actin filaments. *Cell Motil. Cytoskeleton* **64,** 519–530
98. Jiang, X., Kenerson, H., Aicher, L., Miyaoka, R., Eary, J., Bissler, J., and Yeung, R. S. (2008) The tuberous sclerosis complex regulates trafficking of glucose transporters and glucose uptake. *Am. J. Pathol.* **172,** 1748–1756
99. Choi, J. H., Bertram, P. G., Drenan, R., Carvalho, J., Zhou, H. H., and Zheng, X. F. (2002) The FKBP12-rapamycin-associated protein (FRAP) is a CLIP-170 kinase. *EMBO Rep.* **3,** 988–994
100. Kotoulas, O. B., Kalamidas, S. A., and Kondomerkos, D. J. (2006) Glycogen autophagy in glucose homeostasis. *Pathol. Res. Pract.* **202,** 631–638
101. Mortimore, G. E., and Poso, A. R. (1987) Intracellular protein catabolism and its control during nutrient deprivation and supply. *Annu. Rev. Nutr.* **7,** 539–564
102. Singh, R., Kaushik, S., Wang, Y., Xiang, Y., Novak, I., Komatsu, M., Tanaka, K., Cuervo, A. M., and Czaja, M. J. (2009) Autophagy regulates lipid metabolism. *Nature* **458,** 1131–1135
103. Roach, P. J., Depaoli-Roach, A. A., Hurley, T. D., and Tagliabracci, V. S. (2012) Glycogen and its metabolism: some new developments and old themes. *Biochem. J.* **441,** 763–787
104. Ceperuelo-Mallafre, V., Ejarque, M., Serena, C., Duran, X., Montori-Grau, M., Rodriguez, M. A., Yanes, O., Nunez-Roa, C., Roche, K., Puthanveetil, P., Garrido-Sanchez, L., Saez, E., Tinahones, F. J., Garcia-Roves, P. M., Gomez-Foix, A. M., Saltiel, A. R., Vendrell, J., and Fernandez-Veledo, S. (2016) Adipose tissue glycogen accumulation is associated with obesity-linked inflammation in humans. *Mol. Metab.* **5,** 5–18
105. Deng, S. S., Wu, L. Y., Wang, Y. C., Cao, P. R., Xu, L., Li, Q. R., Liu, M., Zhang, L., Jiang, Y. J., Yang, X. Y., Sun, S. N., Tan, M. J., Qian, M., Zang, Y., Feng, L., and Li, J. (2015) Protein kinase A rescues microtubule affinity-regulating kinase 2-induced microtubule instability and neurite disruption by phosphorylating serine 409. *J. Biol. Chem.* **290,** 3149–3160
106. Hurov, J. B., Huang, M., White, L. S., Lennerz, J., Choi, C. S., Cho, Y. R., Kim, H. J., Prior, J. L., Piwnica-Worms, D., Cantley, L. C., Kim, J. K., Shulman, G. I., and Piwnica-Worms, H. (2007) Loss of the Par-1b/MARK2 polarity kinase leads to increased metabolic rate, decreased adiposity, and insulin hypersensitivity in vivo. *Proc. Natl. Acad. Sci. U.S.A.* **104,** 5680–5685
107. Lennerz, J. K., Hurov, J. B., White, L. S., Lewandowski, K. T., Prior, J. L., Planer, G. J., Gereau, R. W. t., Piwnica-Worms, D., Schmidt, R. E., and Piwnica-Worms, H. (2010) Loss of Par-1a/MARK3/C-TAK1 kinase leads to reduced adiposity, resistance to hepatic steatosis, and defective gluconeogenesis. *Mol. Cell. Biol.* **30,** 5043–5056
108. Sun, C., Tian, L., Nie, J., Zhang, H., Han, X., and Shi, Y. (2012) Inactivation of MARK4, an AMP-activated protein kinase (AMPK)-related kinase, leads to insulin hypersensitivity and resistance to diet-induced obesity. *J. Biol. Chem.* **287,** 38305–38315
109. Hurov, J., and Piwnica-Worms, H. (2007) The Par-1/MARK family of protein kinases: from polarity to metabolism. *Cell Cycle* **6,** 1966–1969